Universidad de Concepción

Facultad de Ciencias Físicas y Matemáticas

Departamento de Física

Evolución Química del Cúmulo Globular pobre en metales NGC 6809

Chemical evolution of the Metal Poor Globular Cluster NGC 6809

Tesis para optar al grado académico de Magíster en Ciencias con mención en física

Autor

María José Rain Sepúlveda

Profesor Guía

Dr. Sandro Villanova

Departamento de Astronomía

Universidad de Concepción

Diciembre, 2017

Concepción, Chile

UNIVERSIDAD DE CONCEPCIÓN

Resumen

Facultad de Ciencias Físicas y Matemáticas
Departamento de Astronomía

Evolución Química del Cúmulo Globular pobre en metales NGC 6809

por María José Rain

NGC 6809 es un Cúmulo Globular que se encuentra ubicado en el Halo de nuestra Galaxia. Dada su edad, NGC 6809 es un perfecto candidato para estudiar la evolución química y la historia de la formación estelar de la Vía Láctea. Nuestro principal objetivo es realizar un estudio espectroscópico lo más preciso posible. En esta tesis presentamos el analisis químico de 11 estrellas gigantes basado en espectros de alta resolución. Los datos fueron obtenidos de la plataforma ESO Science Archive y provienen del espectrógrafo FLAMES/UVES montado en UT2 en el telescopio VLT. Utilizando dos tecnicas: Ancho equivalente (EW) y espectrośintesis, derivamos las abundancias de los siguiente elementos químicos: O, Na, Mg, Al, Si, Ca, Ti, V, Cr, Mn, Fe, Co, Sc, Ni, Cu, Zn, Y, Zr, Ba, La, Ce, Eu, Nd y Dy. Encontramos una velocidad radial heliocéntrica de 174.7 $\pm$ 3.2 km s^{-1} y un contenido de Hierro de [Fe/H]=-2.01 $\pm$ 0.02 (error en el promedio). Encontramos un enriquecimiento α de 0.40 $\pm$ 0.04 que corresponde a un valor típico de los Cúmulos Globulares en este rango de metalicidad. Una gran dispersión es observada en las abundancias de los elementos livianos O, Na, Al y Mg confirmando la presencia de una anticorrelación entre Na-O y Mg-Al. No encontramos ningún tipo de variacion en los elementos iron-peak ni en los elementos pesados.

UNIVERSIDAD DE CONCEPCIÓN

Abstract

Facultad de Ciencias Físicas y Matemáticas
Departamento de Astronomía

Chemical Evolution of the Metal Poor Globular Cluster NGC 6809

by María José Rain

NGC 6809 is a metal-poor Globular Cluster located in the Halo of our Galaxy. Due to its age, NGC 6809 is a perfect candidate to study the chemical evolution and star formation history of the Milky Way. We aim to perform an accurate spectroscopic study of the cluster in order to search for Multiple Populations. We present abundance analysis of 11 giant stars based on high-resolution spectra. The data from FLAMES/UVES instrument mounted on UT2 at VLT telescope was obtained from the ESO Science Archive. By using two techniques: Equivalent Width (EW) and Spectrum-Synthesis, we derived abundances of elements like O, Na, Mg, Al, Si, Ca, Ti, V, Cr, Mn, Fe, Co, Sc, Ni, Cu, Zn, Y, Zr, Ba, La, Ce, Eu, Nd and Dy. We found a radial velocity of 174.7 ± 3.2 km s^{-1} and a mean iron content of [Fe/H]=-2.01 ± 0.02 (error on the mean). We find a α- enhancement of 0.40 ± 0.04 typical of Halo Globular Clusters in this metallicity regime. A large spread is observed in the abundances of light elements O, Na and Al confirming the presence of a Na-O and Mg-Al anti-correlation and a Na-Al correlation. We did not find sings of variations in iron-peak and heavy elements.

Contents

List of Figures

List of Tables

Chapter 1

General Introduction

The importance of Galactic Globular Cluster (GGCs) is that they are a good representation, as first aproximation of what we call a simple stellar population (SSP), this terminology was suggested to highlight theoverall property of a population in which stars show similar characteristics in terms of age and metallicity. In fact, a SSP is assumed to be originated in a single star formation episode from a cloud with an homogeneous chemical composition. In this sense GCs are excellent candidate for testing and calibrating stellar evolutionary model. However this approximation does not hold when you look them in more details. The fact that GCs are not formed by a single stellar populations should be evident, since instantaneous star formation and complete chemical homogeneity of the original molecular cloud are not to be expected. Rather, multiple populations in globular clusters provide information on how they formed, and on the likely relation with the host galaxy, these clusters As the oldest population objects for which accurate ages can be inferred, they place an important constraint on the age of the Universe and, in turn, on cosmology. GCs are one of the best and powerful ways to study and to understand the chemical evolution and star formation history of our Galaxy. In particular, globular clusters (GC) are among the oldest known objects in the Universe that's why they are considered as fundamental benchmarks for testing stellar evolution models and for population synthesis model.

1.1 Globular Clusters properties

Globular clusters (GCs) are compact objects, they typically contain between 10^4 to 10^6 stars with a spherical distribution, the total mass of this objects is of the order $10^5 M_\odot - 10^6 M_\odot$. This type of cluster are really bright with integrated luminosity (M_V) ranging between -5 to -10. They have a very small core radius of $\sim$1 pc, this means

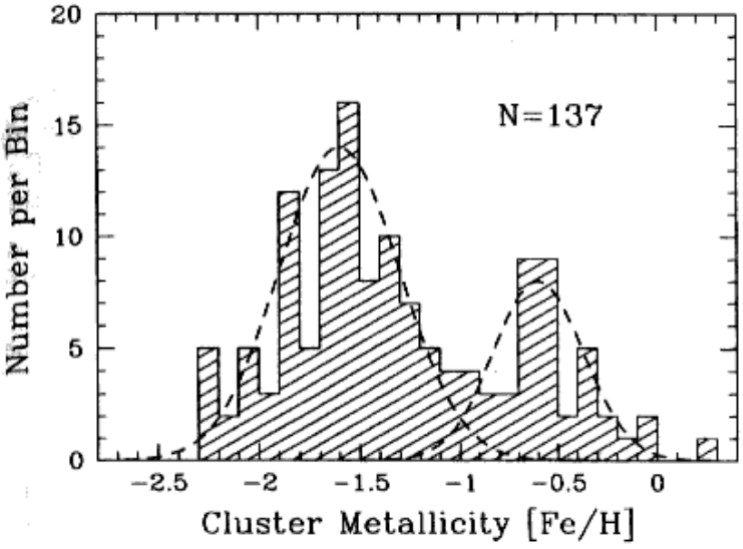

FIGURE 1.1: Metallicity distribution of Milky Way Globular Clusters. Source: Harris (2001).

that the central density of this cluster is extremely high (10^5 stars pc^{-3}). In the Milky Way (MW) they spand over a wide range of metallicity -2.5 <[Fe/H]< 0. These objects are essencially older than 10^{10} years in the MW which means that they formed in the very early stages of the life of our Galaxy. Due to his age they are found only in the old populations: the Halo, Thick Disk and Bulge, but not in the Thin disc. There are $\sim$ 150 Globular Clusters in the Milky Way orbiting the Galaxy about the Galactic center, with orbits in random orientations, unlike Open Clusters which follow the Galactic rotation. Their spatial distribution in the Galaxy is showed in Figure 2.2.

If we look at the [Fe/H] distribution of Milky Way globular clusters it is possible to distinguish two peaks (see Figure 1.1). The two peaks are at $\sim$-1.50 and $\sim$-0.50 dex. These peaks basically represent two systems: the first peak represent Halo clusters and the second peak represent Thick disc or Bulge clusters. The Thick-disk or Bulge clusters have a flattened spatial distribution and rotate about the Galactic Center while the Halo clusters have little net rotation and spherical distribution.

1.2 Chemical Patterns

Every Galaxy is characterized by a chemical enrichment history which is driven by the nucleosynthesis occurring in different generation of stars where chemical elements heavier than He are build up with different processes on different timescales. Stars are able to synthesize different elements through different channels and to release a fraction of them (the so-called yields) at different epochs from the star formation onset, not only at the end of their lifetimes (e.g. as Supernovae) but also during their evolution (e.g. through wind

activity from AGB stars, fast rotating massive stars). When this material is released it is mixed with the interstellar medium (ISM) and a new stellar generation can form from this pre-enriched material. In particular, investigating the chemical composition of the GCs stars is extremely important, because these are fossils of the earliest epoch of the galaxy chemical evolution history. The different chemical elements ratios are powerful to study the initial mass function (IMF) and the star formation rate (SFR), since the material ejected by the stars (yields) of a given element depends on the relative frequency of stars of different masses born in a stellar generation and on the corresponding metal ejected by these stars. Chemical analysis of GCs stars is useful for flagging the timescales of chemical evolution.

1.2.1 Alpha elements

The alpha process, is one of the two classes of nuclear fusion reactions by which stars convert helium into heavier elements. The name α elements is due to the fact that these elements are formed through α-capture processes on seed nuclei. The α particle consists in a nucleus of Helium made of two protons and two neutrons. The main elements belonging to this family are O, Ne, Mg, Si, S, Ca, and Ti are progressively built up starting from the burning of He, C and Si in the case of Ti (Woosley & Weaver, 1995).

Enhancements of alpha elements in metal-poor stars were first identified by Aller & Greenstein (1960) and more firmly established by Wallerstein (1962), who found excesses of Mg, Si, Ca, and Ti relative to Fe. The trend for the α elements as a function of [Fe/H] in our Galaxy shows two different regimes (see Figure 1.2): for -1.0 $<$ [Fe/H] $<$ 0.0 dex, the [α/Fe] ratio increases as the metallicity decreases, reaching a factor of 2-3 above solar (i.e., [α/Fe] $\sim$ 0.3 dex) at [Fe/H] $\sim$ -1 dex, while for [Fe/H] $<$ -1 dex the [α/Fe] ratio remains almost constant.

The elements produce by massive stars are released into the ISM at the end of the stellar life during supernovae explosions and according with the stellar evolution theory α-elements are mostly synthesized in massive stars. Type Ia supernovae (SNIa) produce mostly iron-peak elements and a little amount of α-elements (e.g Nomoto et al., 1984) while Type II supernovae (SNeII) mainly produce α-elements and little of iron-peak elements (e.g Woosley & Weaver, 1995). It was suggested by Tinsley (1979) that the α trend is due to the time delay between the explosions of SNII and SNIa. Thus, after the delay for the onset of SNIa, the [α/Fe] ratio decreases from the value set by the SNII ejecta.

In Figure 1.2 is possible observed a "knee", the position of this knee marks the metallicity reach by the system in the epoch when SNIa start to dominate, this knee depends of

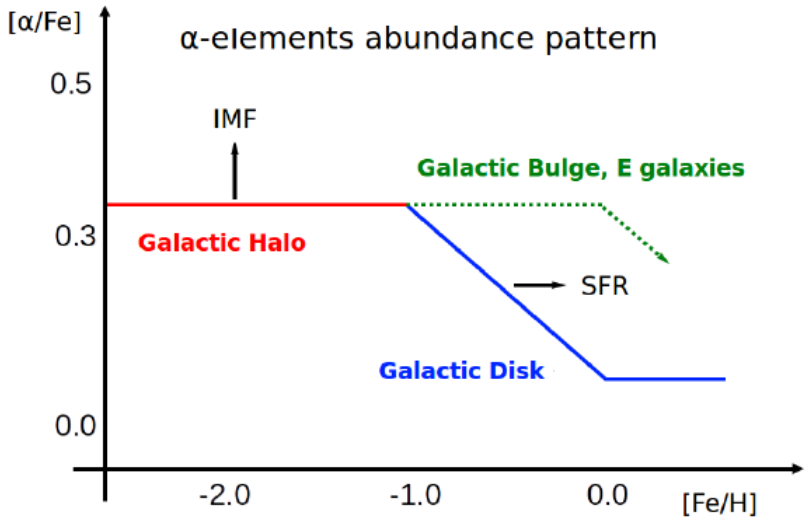

FIGURE 1.2: α/Fe trend of the Milky way. Source: McWilliam et al. (1995)

the SFR. For example when the SFR is high, the gas reached larger [Fe/H] before the ejecta of SNIa are fully mixed into ISM and the position of the knee will be at a higher [Fe/H]. A little change of the IMF determines an increase or decrease of the number of high-mass stars formed, which explode as SNII, as a consequence this corresponds to different amount of α elements produced.

1.2.2 Light elements

By comparing the ranges of element abundances in field and Cluster stars, we see that large variations (at the same metallicity) are restricted to the dense environment of globular clusters and mainly concern light elements. The first indication of variations in the light elements was found by Osborn (1971). In his work he found different N content in two stars in the clusters M5 and M10 (see Figure 1.3). A couple of years later different distribution on CN and CH bands were found by several authors (e.g Zinn, 1977). Norris (1987) found that almost all the studied GCs display either a bimodal or multimodal CN distribution (see Fig. 1.4). Today, is well know that CN and CH bands are anti-correlated, with CN-strong stars also characterised by weak CH absorption and vice versa; i.e. N is found to be anti-correlated with C.

The variations of C and N are not the only one present in GC. The Lick-Texas group found that stars with larger CN indices also have larger Al abundances, larger Na abundances, and lower O abundances than stars with lower CN indices. In particular they found that the light elements Na and O are anti-correlated (see Fig. 1.5). An evolutionary mixing was proposed by Denisenkov & Denisenkova (1990) as the main cause of these inhomogeneities. The authors considerer that a normal stellar evolution may contribute

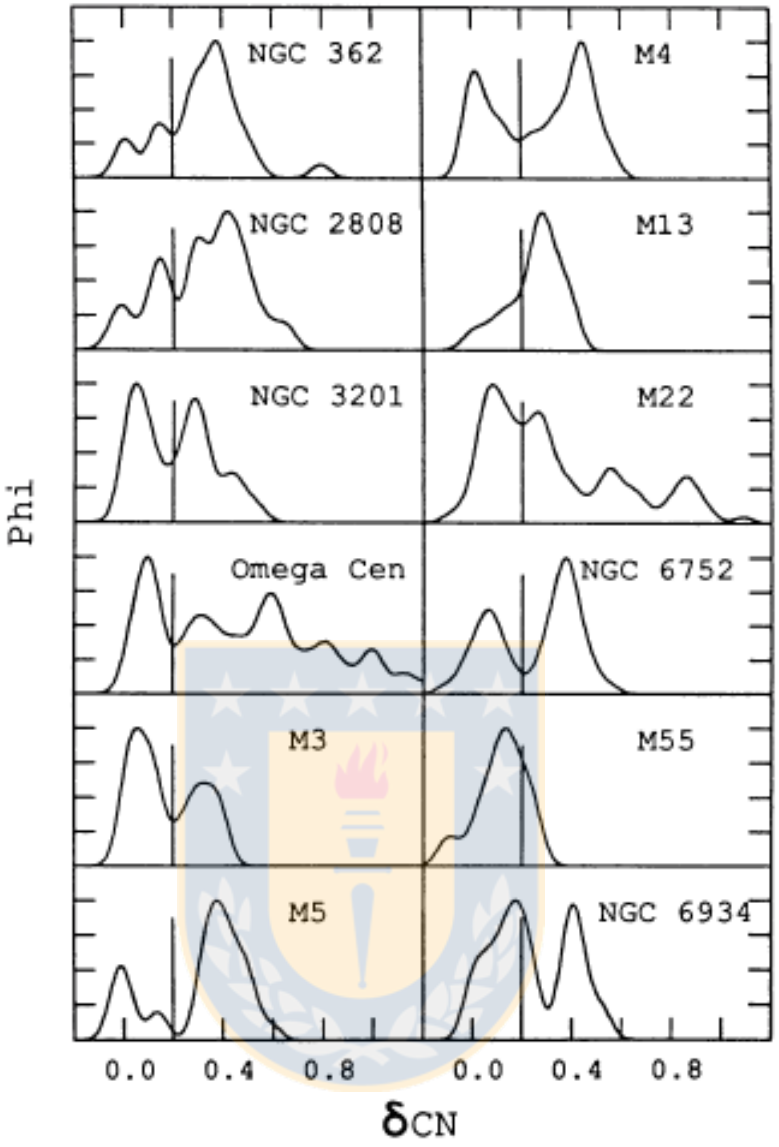

FIGURE 1.3: Members of M5 are shown as triangles and members of M10 are shown as crosses. Two star show a clear N-enhancement. Source: Osborn (1971).

to the observed anti-correlations in evolved RGBs and that the origin of these variations is the result of proton capture reactions in the hydrogen burning shell at high temperature, where several synthesis chains are simultaneously active: CNO cycle, NeNa and Mg-Al chains (Denisenkov & Denisenkova, 1989), for more information about these process see subsection 1.3.

At the beginning, the spectroscopic studies using high resolution spectra were limited just to the brighter red giant stars. A major step forward resulted from the advent of high-resolution spectroscopy on 8-10 meter class telescopes (e.g FLAMES/UVES), which allowed a detail chemical study of turnoff main sequence stars in the brightest GCs. Gratton et al. (2001) found variations in C, N, O, Na, Mg and Al in MS stars (turn-off

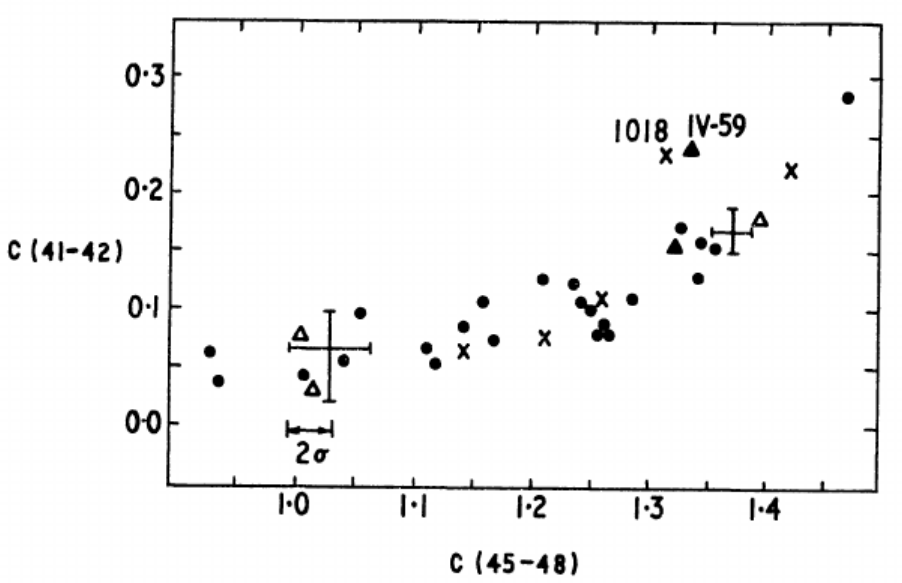

FIGURE 1.4: Bimodal distribution in CN distribution for the GCs M5 and M10. The two anomalous stars are mark with their respective ID. Source: Norris (1987).

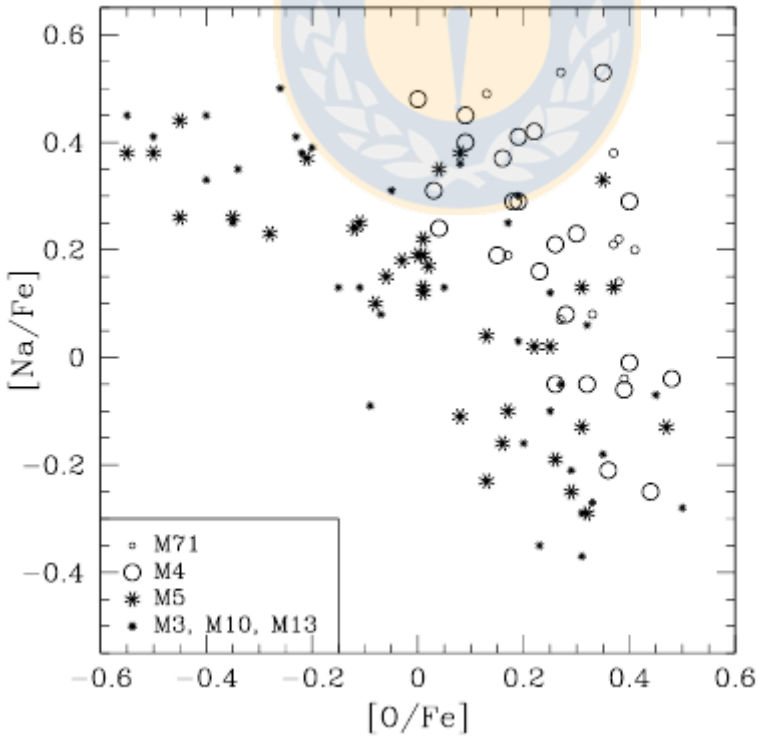

FIGURE 1.5: [Na/Fe] versus [O/Fe] plots for M5 and M4 and globular clusters previously studied by the Lick-Texas group. Image taken from Ivans et al. (2001).

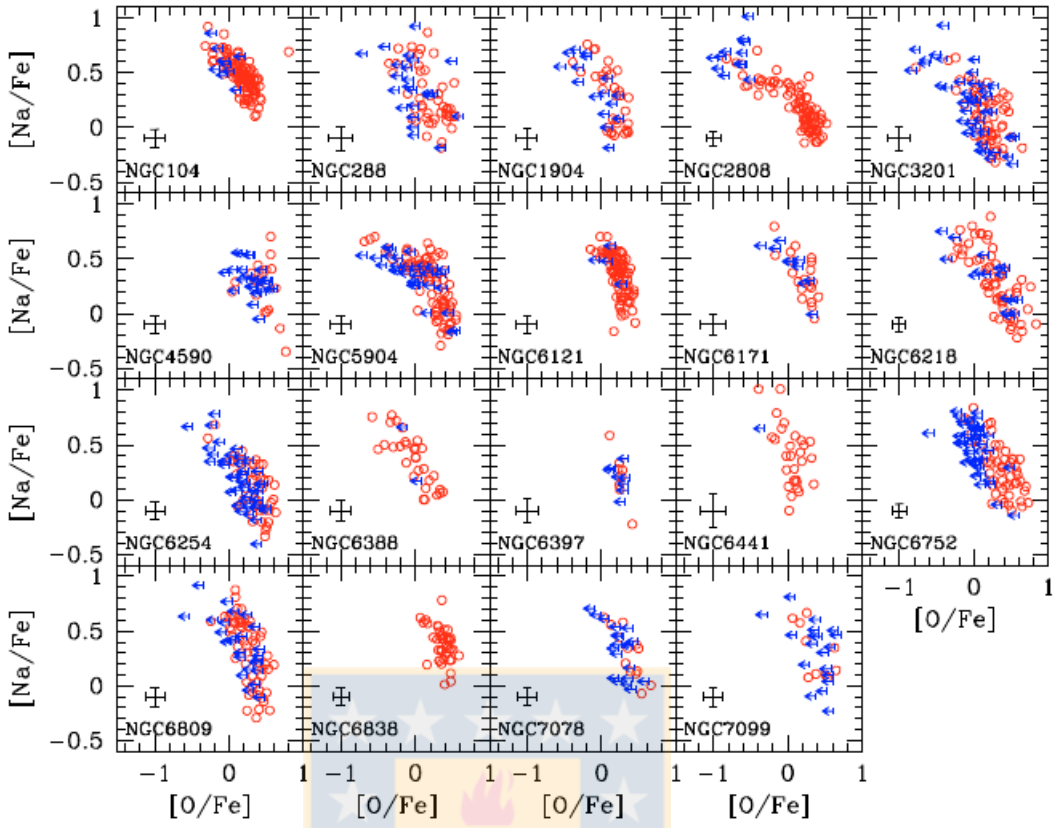

FIGURE 1.6: The Na-O anticorrelation observed in 19 GCs. All stars with Na and O abundances from GIRAFFE and UVES spectra are used. Star-to-star error bars are indicated in each panel. Upper limits in O abundances are shown as detections are indicated as open circles. Source: Carretta et al. (2009)

and early sub-giants stars). From there on, these patters have been convincingly detected down to the sub-giant branch (SGB) and the MSTO (e.g Ramírez & Cohen, 2002) in many clusters.

The work of Cohen et al. (2002) show that the observed spread in light elements are quite similar between MS and SGB stars. This finding imply that mixing theories cannot explain the abundance anomalies seen among non evolved stars, because the whole star, not only the outer convective envelope, is polluted. MS star are characterised by negligible outer convective zones. Even if sufficient mixing could be achieved during MS evolution, it would also result in changes in helium abundances and extended lifetime of stars, e.g. mixing would result in broadening the MSTO region in the CMD, contrary to what observed. The required temperatures are high ($>$ 10 - 40 $\times$ 10^6K for the CNO and NeNa cycles, and even higher for the MgAl cycle, T $>$ 70$\times$$10^6$ K), and cannot be reached in the interior of the presently observed GC low mass stars (Prantzos et al., 2007). Hence, the abundance anomalies are not produced in the course of the evolution of stars we are currently observing but they were produced elsewhere, potentially in the interiors of more massive stars.

While a first generation (FG) of stars shares the halo field stars composition, the second generation (SG) show variations in light elements (specifically Na-enriched and O-depleted, for more information about the Na-O anti-correlation see Subsection 1.2.2.1) that are unique in every GC. Stars of the later generations formed from material expelled by FG stars (**the polluters**) mixed with pristine material Prantzos & Charbonnel (2006) (for information about the polluters see 1.4).

1.2.2.1 Na-O anticorrelation

Figure 1.6 shows the Na-O anti-correlation observed in nineteen Galactic GCs with FLAMES/UVES on VLT by Carretta and collaborators. They found this anti-correlation everywhere and also define this signature to be fundamentally related to the mechanisms of formation and early evolution of GCs. Due the homogeneity of the study they used the abundances measured to provide a chemically tag of multiple stellar populations and used them to separate and quantify the fraction of first and second-generation stars in GCs. An important fact to mention here is that this signature is absence in some GCs (e.g Rup 106, Villanova et al., 2013), especially in those with low mass(see Fig. 1.7). This had led to the notation that GCs host multiple populations (MPs).

This feature is different in every galactic GCs. In Fig. 1.8 we show two GC hosting the Na-O anti-correlation. The distribution are quite different, in the case of NGC 6121 there is a large variation in Na but not in O. In NGC 2808 instead shows a wide variations both in O and in Na.

By using a dilution model it is possible to shed more light on the pristine O and Na abundances of FG stars. The basic idea is to use initial composition of the cluster and then to adding polluted material in order to determine the slope of the O-Na anti-correlation by using the minimum O and maximum Na abundances in each cluster. The dilution model was useful to probe that these anti-correlations differ systematically from cluster to cluster. Additionally in every dilution model, the maximun O and mininum Na of each cluster reflects the composition of fields Halo stars.

Along the Na-O anticorrelation it is possible to identified a primordial (P) component, with stars populating the placed occupied by field stars of similar metallicity, showing only the chemical pattern from supernovae nucleosynthesis. This component is present in all clusters, corresponding to an average of 30% up to 50% (only in a few cases). The remaining stars are SG. Carretta et al. (2009) could separate this SG into an intermediate (I) and extreme (E) populations (see Fig. 1.9). It is possible to find most of the stars in the I component (up to 60–70% of currently observed cluster stars). The E population is not present in all clusters and is more easily found in very massive clusters.

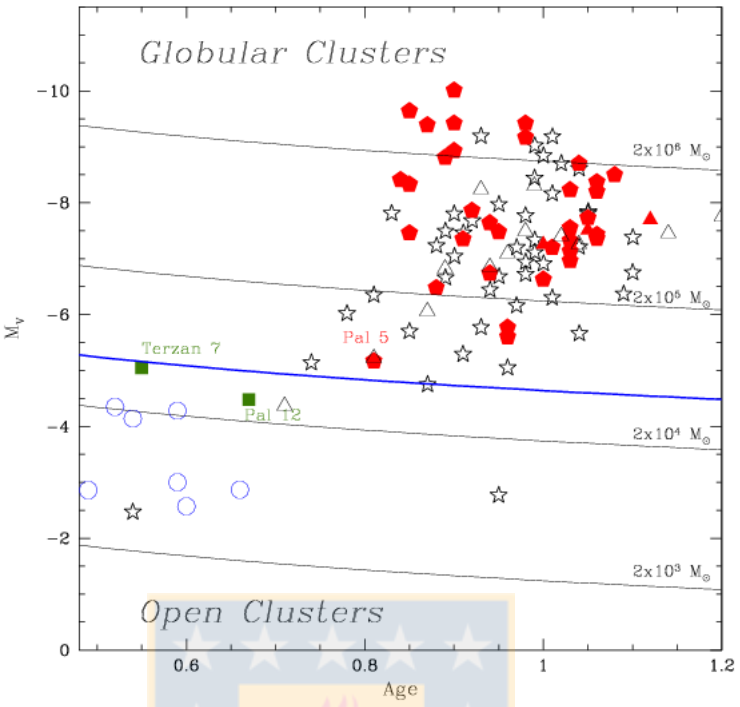

FIGURE 1.7: Relative Age parameter vs absolute magnitude MV for globular and old open clusters. Red filled pentagons and triangles are GCs where Na-O anticorrelation has been observed, in the Milky Way or the LMC respectively; green squares are clusters which do not show evidence for O-Na anticorrelation, both members of Sagittarius dSph, either of the main body (Terzan 7) or the stream (Pal 12). Open stars and triangles mark clusters for which not enough data is available, in the Milky Way or the LMC respectively. Finally, open circles are old open clusters. Source: Carretta et al. (2010)

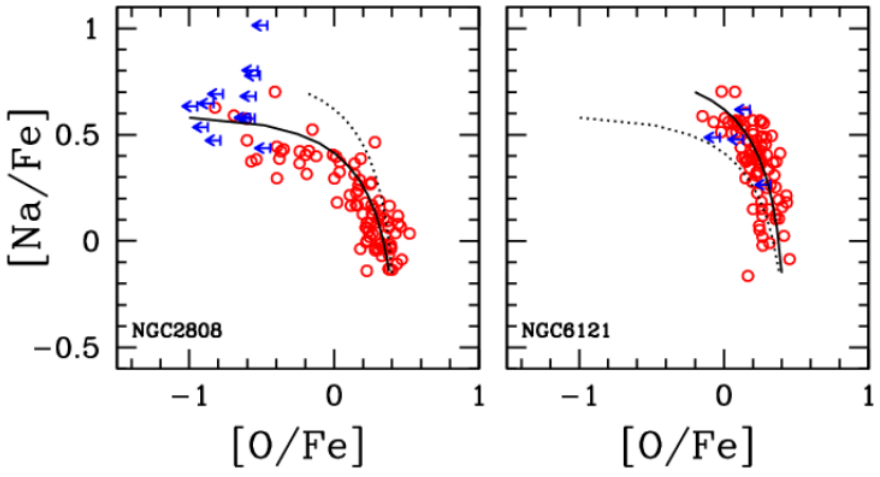

FIGURE 1.8: Na-O anticorrelation for two globular clusters. Left: NGC 2808 and Right: NGC 6121. The corresponding dilution model are plot in both sides. Source: Carretta et al. (2010).

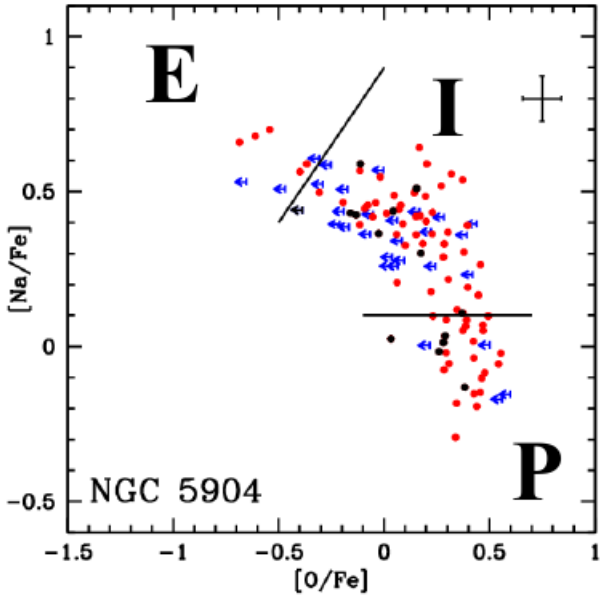

FIGURE 1.9: Na-O anticorrelation for NGC 5904. Lines separate the primodial, intermediate and extreme components. Source: Carretta et al. (2010).

The Na-O anticorrelation varies from cluster to cluster and seems to depend on the absolute magnitude of GCs, which reflects their total mass Carretta et al. (2009). According to Carretta et al. (2010), the lower limit for a GC to exhibit the O-Na anticorrelation is a present-day mass larger than a few 10^4 $M_\odot$.

1.2.3 Iron-peak elements

Iron peak elements are a group of elements with atomic number $22 < Z < 28$ and atomic masses (A) about 40 to 60 that are synthesized by the silicon burning process and appear in the iron peak. They are mainly Iron (Fe), Chromium(Cr), Manganese (Mn), Cobalt (Co), Nickel (Ni), Scandium (Sc), Zinc (Zn), Copper (Cu) and Vanadium (V). These elements are mostly produced during the explosive nucleosynthesis associated to SNIa, but some contributions from the weak s-processes in massive stars (e.g. for Cu) and from SNII have been also proposed (e.g. for Fe, Cu and Zn)

Iron is the best known chemical element due to the huge number of available atomic transitions over the whole spectral range, and at all the metallicities, it has been extensively studied in almost all astrophysical contexts. There are no nuclear reactions able to alter the iron abundance of a star. Since Iron has only two main formation channels: SNII and SNIa and both release into the ISM tenths of solar masses of iron and iron-peak elements. Because of this, all abundance ratios are usually expressed in terms of iron content.

Scandium and Vanadium closely follow solar values. Gratton & Sneden (1991) found [V/Fe] $\sim$ 0.0 and Gratton & Sneden (1991), McWilliam et al. (1995) found [Sc/Fe]=0.0. Zhao & Magain (1990) found that the [Sc/Fe] is slightly supersolar in metal-poor dwarfs. For Mn the picture is different. [Mn/Fe] for -1.0 $<$ [Fe/H] $<$ 0.0 dex show overabundances of $\sim$ 0.30 dex. While for -2.5 $<$ [Fe/H] $<$ -1.0 dex remains constant at -0.40 dex for field stars. Very similar to that of [Mn/Fe] is the behaviour of [Cr/Fe], which is found to increase with the metallicity.[Ni/Fe] is usually found to be close to the solar value over the entire metallicity range, suggesting that the origin of Ni is strictly linked to that of Fe from both SN types. [Co/Fe] is found to increase as metallicity decreases, it seem that the main contribution in the production of Co comes from SNII McWilliam et al. (1995). Sneden et al. (1991) and Bensby et al. (2005) found that [Cu/Fe] decreases with metallicity and Zn is roughly constant at [Zn/Fe] = 0.0 dex for all metallicities. According with Cayrel et al. (2004) [Zn/Fe] rises steeply to $\sim$ +0.5 at the lowest metallicities.

The chemical homogeneity in iron peak is a representative feature in most of the GCs. However, star-to-star [Fe/H] spreads have been found in the most massive GCs, both in the Milky Way and in dwarf spheroidal galaxies. The Globular Cluster ω Cen shows the larger variation which covers more than 1.5 dex Villanova et al. (2014).

1.2.4 Neutron-capture Elements

These elements are mainly produced by neutron capture (n-capture) reactions through the s-process and the r-process. When a neutron decays into a proton, a new nucleus with a higher atomic number is formed. The captured is considered to be slow if the timescale for the neutron capture is large compared to the timescale of the nuclear decay, this is the case of the s-process. In the case that the neutron capture is rapid compared with the timescale of the decay, we have the r-process. Both processes happen in a different physical condition and are likely to happen in different astrophysical sites too. While the s-process occurs primarily in AGB stars, the r-process occurs in SNII explosions. The typical s-process elements observable in the stars are Sr, Y, Zr, Ba, and La, while the main chemical element produced through r-process is Eu.

In the lower metallicity range the amount of r-elements in stars is clearly supersolar, reaching values up to +1.5 dex for [Eu/Fe] (Barklem et al., 2005). With the increase of [Fe/H] these abundances decline reaching a [Eu/Fe] $\sim$ 0.0 dex at solar metallicity.

The production of s-elements ocurr in the neutron-capture reactions during the thermal pulses of AGB stars. In the lower metallicity range a large number of neutrons is available for a limited amount of seed nuclei, this would result in a larger number of captures, thus favoring the production of heavy (A$>$130) s-elements (e.g La and Ba). When the

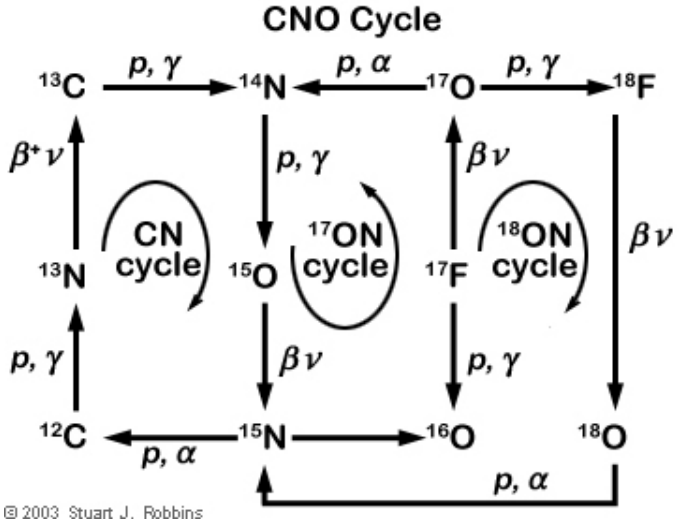

FIGURE 1.10: CNO cycle. This diagram shows three different cycles that feed into each other, separated by the two catalysts that are used - C and N, ^{18}O and N, or ^{18}O and N. In this diagram, ρ is used to indicate a proton while α indicates a helium nucleus (also known as an "alpha particle"). Source: Stuart J. Robbins 2003.

metallicity increase, the number of aailable seed nuclei increase too and the number of neutron captures decreases, thus favoring the formation of light s-elements belonging to the group of Sr, Y, and Zr (A $\sim$ 90). For these reason we can say that the production of s-elements occur in a metallicity-dependent way. In the Milky Way [s-process/Fe] ratio increases with the metallicity.

Heavy elements Barium and lanthanum in ω cen increase with iron for stars with [Fe/H]<-1.5 (Marino et al., 2011) showing a significant spread. Other GCs showing evidence of of and internal dispersion of neutron-capture elements are: NGC 6229 (Johnson et al., 2017), NGC 5824 (Roederer et al., 2016), NGC 6273 (Johnson et al., 2016).

1.3 Origin of the abundance anomalies

According to Denisenkov & Denisenkova (1990), Prantzos & Charbonnel (2006), Prantzos et al. (2007) the anticorrelations among light elements are the result of H-burning through the CNO-cycle and the NeNa, Mg-Al chains.

1.3.1 CNO-cycle

In the case of the CNO cycle, ^{12}C nucleus is used as catalysts for hydrogen-to-helium fusion. The CNO cycle is a process of stellar nucleosynthesis in which stars on the Main Sequence fuse hydrogen into helium. The cycle results in the fusion of four hydrogen

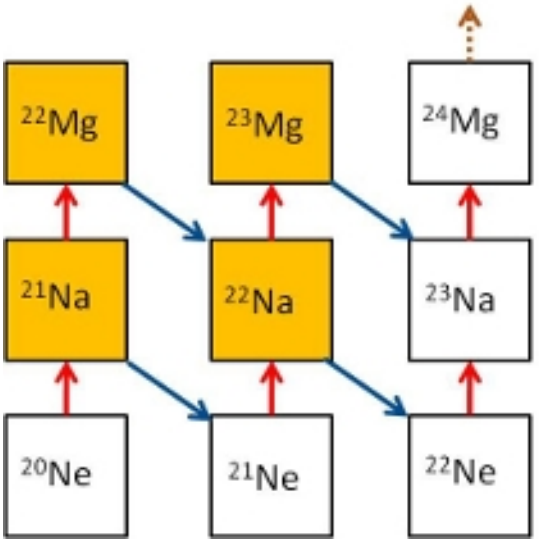

FIGURE 1.11: NeNa chain. Red arrows denote proton captures, blue arrows denote β-decays. Source: https://www.nucastro.ph.tum.de

nuclei (^{1}H, protons) into a single helium nucleus (^{4}He, alpha particle). The cycle start once the stellar core temperature reaches 14×10^{6} K and is the primary source of energy in stars of mass M $>$ 1.5 $M_{\odot}$. Stars of lower mass convert hydrogen to helium via an alternative process known as the 'proton-proton chain'. In figure 1.10 it is schematized the complete cycle, this process follow: A ^{12}C nucleus captures a proton and emits a gamma ray, producing ^{13}N. ^{13}N is unstable and emits a beta particle, decaying to ^{13}C. ^{13}C captures a proton and becomes ^{14}N via emission of a gamma-ray. ^{14}N captures another proton and become ^{15}O by emitting a gamma-ray. ^{15}O becomes ^{15}N via beta decay. ^{15}N captures a proton and produces a helium nucleus (alpha particle) and ^{12}C, which is where the cycle started.

1.3.2 NeNa chain

The NeNa cycle of hydrogen burning allows the conversion of four protons into helium using Ne and Na isotopes as catalysts. The NeNa cycle is not a very strong source of energy for stars. Its importance lies, however, in the fact that it allows the synthesis of the elements between ^{20}Ne and ^{24}Mg. The cycle start once the stellar core temperature reaches 35×10^{6} K. In figure 1.11 it is schematized the complete cycle. Starting with proton capture on the seed ^{20}Ne, there are two ways to produced ^{22}Na can be produced after proton capture onto ^{20}Ne: i) proton capture onto ^{21}Na to ^{22}Mg, followed by β-decay to ^{22}Na ii) β-decay from ^{21}Na followed by proton capture onto ^{21}Ne. Furthermore, ^{22}Na is itself destroyed by proton capture to ^{23}Mg.

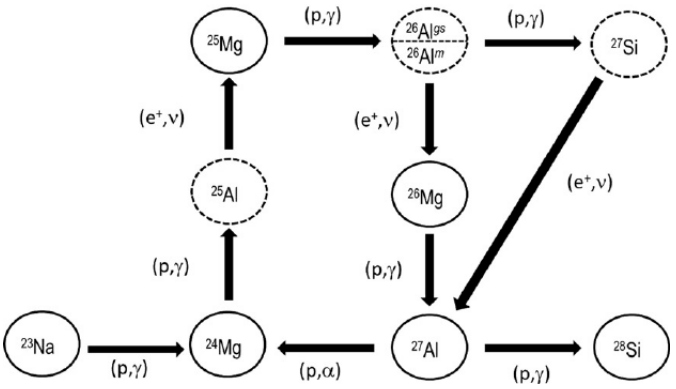

FIGURE 1.12: MgAl chain. Solid and dashed lines refer to stable and unstable isotopes, respectively. Source: http://inspirehep.net/record/1204574/plots.

1.3.3 Mg-Al chain

The Mg-Al chain start once the stellar core temperature reaches really high temperatures: $\sim 70 \times 10^{6}$ K. The first isotope in the Mg-Al chain to be affected is ^{25}Mg, which is burnt to ^{26}Al. The β-decay lifetime of ^{26}Al relative to proton capture generally favours proton capture within the H-burning shell. This produces the unstable ^{27}Si which quickly β-decays (with a lifetime on the order of a few seconds) to ^{27}Al. The abundance of ^{26}Mg is enhanced by the β-decay of ^{26}Al in the H-shell ashes. In figure 1.12 it is schematized the complete cycle

1.4 GC self-enrichment: Polluters

For a long time the main question was to know if such patterns were inherited at the birth of the stars that we are currently observing (the so-called self-scenario hypothesis) or if they were generated in the course of the evolution of these objects (the so-called evolution hypothesis). The discovery of the anti-correlations in main sequence (MS) stars (Gratton et al., 2001) has given a new spin to the self-enrichment scenario. Indeed turnoff stars are not hot enough for the required nuclear reactions to occur in their interiors. This implies that the O, Na, Mg and Al abundance anomalies pre-existed in the material out of which these objects formed; their gas must have been polluted early in the history of the cluster by more massive and faster evolving stars. In this context, FG stars must be born with the original composition, while SG stars formed from the pristine gas polluted by hydrogen-burning processes material ejected by FG stars.

Several stellar types have been proposed as candidate polluters, because they reach extreme temperatures within their interiors, in the following subsection we are going to discuss about these stars.

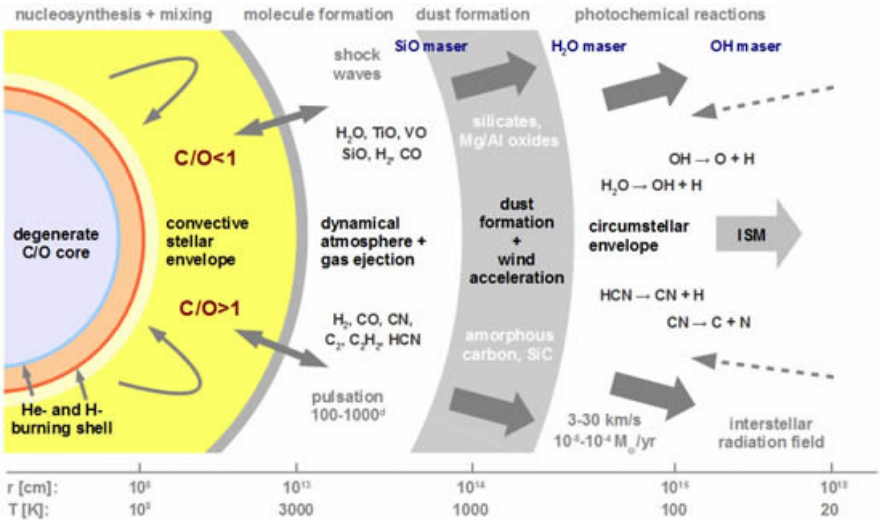

FIGURE 1.13: Schematic chemical structure of the circumstellar shell of an AGB star. Source: https://www.asiaa.sinica.edu.tw

1.4.1 Asymptotic Gian Branch stars (AGB)

The lifetime of intermediate mass AGB stars is relatively short between 50-100 Myr, they do not produce alpha or iron-peak elements and possible they experience the hot bottom burning (HBB) that processes the material included inside their large convective envelopes through CNO, NeNa and MgAl nucleosynthesis. This qualitative advantages have been placed massive AGB stars ($\sim$ 5 - 10 $M_{\odot}$) as the first stellar sources of the origin of GC self-enrichment. This scenario has been proposed and discuss by several authors (e.g Cottrell & Da Costa, 1981, D'Antona et al., 2002, Decressin et al., 2009, Ventura et al., 2001).

For the basic scenario we considerer that the stars in the new cluster share the same age and abundances pattern, i.e they are a simple stellar population. This stars represent a first/primordial generation (FG). After $\sim$ 50 Myr, the first generation of stars begin to evolve through the AGB phase of stellar evolution, an the winds of these stars, due to their low velocity are not able to escape the cluster. This material concentrates in the center of the cluster and a new generation of stars begins to form out of this material (second generation of stars, SG). A prediction of this scenario is that all the pristine material that remain after the formation of the first generation of stars is lost from the cluster together with the associated SNe ejecta before the second generation of stars formed. Then that external pristine material is re-accreted from the surroundings by the GC after the SNe phase, and mixed with AGB ejecta to form a SG of stars.

These model fails on explain the observed chemical patterns observed in today GC stars. If a stellar population/generation forms directly from the ejecta of massive AGB stars, it should show: a correlation between Oxygen and Sodium, C+N+O enrichment with

respect to FG stars, Mg-depleted stars should be Na-poor, and all SG stars should have similar and relatively high helium.

The composition of the material ejected by AGBs through winds critically depends on what mechanism dominates. Third dredge-up (TDU) brings to the stellar surface primary C, O and Ne. Mg is produced via successive α-captures on N, this production takes places in He-burning shell (HeBS) at $\sim 3\times 10^8$ K (Al isotopes are not produced in the HeBS). HBB modifies the envelope abundances via the CNO-cycle and the NeNa and MgAl-chains. When the NeNa and MgAl chains operate at higher temperature, Na and Al are produced thanks to the dredged-up of Ne and Mg respectively. But in the case of very high HBB temperatures, both Na and Mg are deplete through proton-capture reactions (e.g Denissenkov & Herwig, 2003). Their models confirm the result of the full models that high HBB temperatures do not favor the Na production that would be required to explain the O-Na anti-correlation in GC stars. Additionally, is not possible to obtain simultaneous O depletion and Na enrichment and keeping the C+N+O sum constant in AGB stars. This is one of the strongest nucleosynthetic arguments against AGB stars being GC polluters since the sum C+N+O increases due to 3DUP. Additionally He-rich material is mixed into the surface via the SDU (not necessary related to the change in light elements, as these elements are processed at different moments of the evolution of the stars and by different mechanisms: TDU and HBB). Ventura & D'Antona (2011) predicted that the He content of the ejecta increase with stellar mass, and can reach He values up to Y$\sim$ 0.38 in high-mass AGB stars. This was confirmed two years later by Ventura et al. (2013). However, this helium content is less than that observed in some GCs.

1.4.2 Fast Rotating Massive stars (FRMS)

It was proposed by Decressin et al. (2007) that Fast Rotating Massive stars could be at the origin of GC abundance patterns. In Fig. 1.14 we plot the schematic view of the evolution of FRMS during their life in the main sequence (MS) proposed by Decressin et al. (2007). Green corresponds to the initial chemical composition, blue and red are the material loaded in H and He burning respectively. At the beginning of the MS a low outflowing equatorial disc forms, on this stage dominates matter ejection with respect to radiative winds (Top panel). Then, when central He-burning start, the composition of the disc material is similar to the observed today in low-mass cluster stars, at this point the star has already lost an important fraction of its initial mass (middle panel). Finally, due to heavy mass loss, the star does not supply its disc anymore and radiative fast wind takes over before the products of He-burning reach the stellar surface and contaminate the slow wind component (bottom panel).

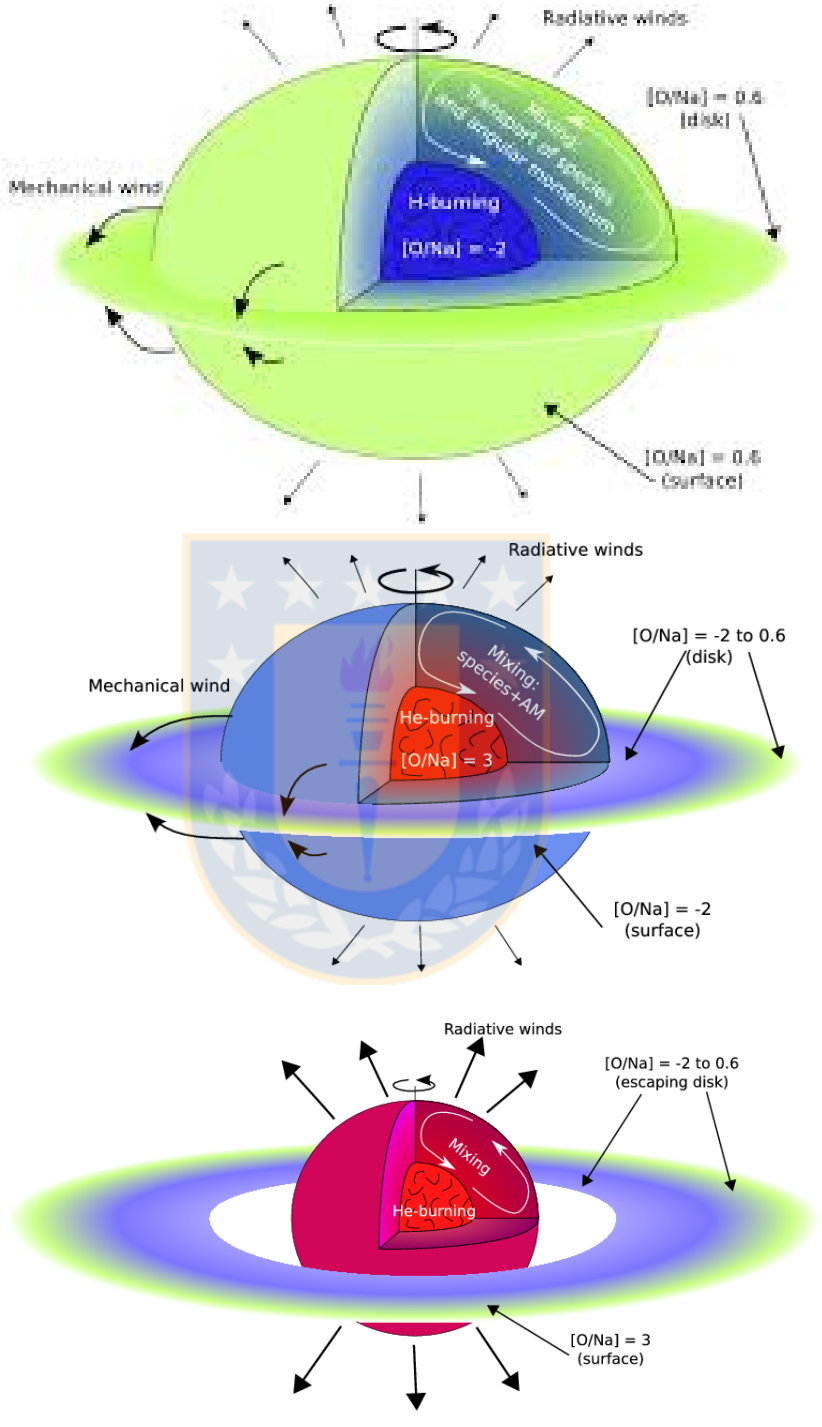

FIGURE 1.14: Schematic chemical structure of an Fast Rotating Massive stars during the main sequence. Source: Decressin et al. (2007).

FRMS scenario is quite similar to that of the AGB scenario, this mean that a SG stars is formed from the enriched material from FG stars. The first difference between this scenario and AGB one is that SG stars to form when the cluster is much younger, typically between 10-20 Myr, so one of the assumptions of this model is that the cluster has retained a relatively large fraction of gas/dust left over from the formation of the FG. This means that the cluster do not have to re-accreted the pristine material from the outside. Just like the AGB scenario the winds of the FRMSs mixes with the left over gas and forms a SG of stars. According with the authors the material ejected in the disc agree with the signatures of of H-burning and presents abundance patterns similar to the chemical anomalies observed in the second generation stars. In the interior of the FRMSs, the anti-correlation O-Na is built up easily, since the CNO and NeNa cycle are active very early on the main sequence.

FRMS are not able to activate the Al-Mg chain before the end of the main sequence (MS), according with Decressin et al. (2007) these objects are able to deplete Mg only if the rate of proton capture in Mg increase by a factor of 1000. Indeed, even in the most massive stars considered in the original FRMS scenario (120 $M_{\odot}$), central temperatures as high as $\sim$75 MK required to decrease Mg are reached only in the second half of the MS. So, FRMS are not able to reproduced the Mg-Al anti-correlation found in some GCs. Also, in this scenario, and unlike AGB scenario, the predicted He enhancement is significantly higher than the value give by the observations.

1.4.3 Binary Stars (BS)

de Mink et al. (2009) by using a model of a binary system between two stars of 20 an 15$M_{\odot}$ investigated the nature of the material expelled by the interaction of the binary system. They found that the star of 20 $M_{\odot}$ lost at least half of its mass and that the chemical pattern produced match the observed trends in GCs. On their models binaries could return enough material to form a chemically enriched SG that is as numerous as the first generation of low-mass stars, without the need to assume a highly anomalous IMF, external pollution of the cluster or a significant loss of stars from the FG.

After 3-8 Myr core collapse SNe begin to explode. This is a problem for scenarios like interacting binary stars which operate in the first few Myr of a cluster's life. The retention of just a small amount of the material will result in Fe spreads that are in conflict with observations (Renzini, 2008).

1.4.4 Very Massive Stars (VMS)

The basic idea of this scenario is that the most massive stars accumulate in the center of the young cluster as a result of dynamical friction. This massive stars collided between them forming a very massive star (VMS) with a mass of $10^4 M_\odot$. This VMS releases hot-hydrogen burning processes through its stellar wind into the intra-cluster environment, this processed material mixes with pristine gas (gas with the same abundance pattern as the initial proto-cluster) and forms further generations of stars until the very massive stars burns out Denissenkov & Hartwick (2014). According to the models of Denissenkov, these objects reach central temperature for CNO, NeNa, and MgAl already at the beginning of the main sequence.

In view of these exploratory studies, VMS can be considered as very promising candidates for GC self-enrichment, at least from the nucleosynthesis point of view. However, many open questions remain about the formation and evolution of these hypothetical star for example, by the end of their MS lifetimes, VMS are expected to reach very high He fractions, that would contradict the observed limits in GCs today. A possible option to explain this He-enhancement is that suggested by Denissenkov & Hartwick (2014), which assume that central H-burning occurs only for a very limited fraction of the main sequence, and ends when the He mass fraction Y has increased by ~ 0.15. This occurs in a few 10^5 yrs, however the biggest problem of this model is the fact that VMSs have not been observed and their existence is still highly speculative.

This thesis is organized as following way: Chapter 1 presents an introduction to the nucleosynthesis sites and channels from which the main chemical elements form. Chapter 2 is focused on the main properties of NGC 6809. In chapter 3 a brief description about the data reduction is given. comparison of our manual-derived chemical abundances and literature results are given in the in chapter 4 and finally, a summary is given in chapter 5.

Chapter 2

The Galactic Globular Cluster NGC 6809

2.1 About NGC 6809

Globular clusters have long been used to study the structure and formation of our Galaxy. NGC 6809, also know as Messier 55 or M55, is a Globular Cluster (GC) in the constellation Sagittarius. It was discovered and cataloged by Nicolas Louis de Lacaille on 16 June 1752 while observing from what today is South Africa. Charles Messier attempted to locate it several times, beginning in 1764, but was frustrated in his attempts because

Figure 2.1: Globular Cluster NGC 6809. Source: www.eso.org

ID	RA_{J2000} (hh mm ss)	Dec_{J2000} (deg mm ss)	l (deg)	b (deg)	R_{sun} (Kpc)	R_{gc} (Kpc)
NGC 6809	19 39 59.71	-30 57 53.1	8.79	-23.27	5.4	3.9

TABLE 2.1: Positional data of NGC 6809. Detail information in the text.

ID	[Fe/H] (dex)	E(B-V)	$(m-M)_V$	M_V	Spectral Type
NGC 6809	-1.94	0.08	13.89	-7.57	F4

TABLE 2.2: Metallicity and Photometry parameters. Detail information in the text.

of the low declination (nearly 31° S) of this object. It never rises sufficiently above the S horizon at Messier's Paris observatory to allow for easy observation (Thompson & Thompson, 2007). He finally observed and cataloged it on the night of 24 July 1778. NGC 6809 is a luminous Globular cluster that is relatively easy to study for many reason, due to its proximity (17.600 light-years away from Earth). This cluster show a typical mass for a GC of about 269.000 times (2.6×10^5) that of the Sun (Boyles et al., 2011) and a unusually low concentration c=0.76 (Trager et al., 1993) makes it relatively easy to collect stellar samples even within the cluster core. Because it is located in the Halo of the Milky Way (See Fig. 2.2) and due of its high Galactic latitude ($b = -23°$), interstellar reddening and contamination is not very high.

However and despite all his good characteristics there are very few studies about it. There are a number of color-magnitude diagrams available in the literature (e.g Alcaino, 1975, Harris, 1975, Lee, 1977, Richter et al., 1999). These studies found similar results indicating that NGC 6809 belongs to the metal-poor, blue-horizontal-branch clusters. Piotto et al. (2015) found that Red Giant Branch sequence in NGC 6809 is split on the ultraviolet CMD, suggesting the presence of two subpopulations. However, spectroscopic evidence speaks rather for chemical homogeneity. Smith & Norris (1982) have obtained low-resolution spectra of a number of giants in NGC 6809. They found that the cluster do not show the bimodal distribution of CN strengths which is typical of many globular clusters. Additionally Pancino et al. (2010) corroborates this behaviour. Both authors believe that this results are most probably owing to the insufficient S/N ratio for the stars in this metal-poor cluster and could indicate that the CN spread might be unusually low in NGC 6809 than in other Clusters. Kayser et al. (2008) found no clear sign of anti-correlation even considering higher S/N giants spectra, questions of CH and CN anti-correlations and of their bimodalitiy in M 55 remains open. On the other hand Carretta (2003), Carretta et al. (2009) found a Na-O anti-correlation present in this cluster which could probe the presence of at least two generations of stars within the cluster (For

ID	V_{rh} (Km/s)	r_c (arcmin)	r_h (arcmin)	Age (Myr)	Mass ($M_\odot$)
NGC 6809/M55	174.7 ± 0.3	1.77	2.23	12.3 ± 1.7	2.7× 10^5

TABLE 2.3: Velocity, age, mass and structural parameters. Detail information in the text.

more information about these variations see Section. 1). On addition Vargas Álvarez & Sandquist (2007) by using the R-method found the highest initial helium abundances (Y=0.27±0.016) for a Globular Cluster, being almost 2σ away from the predicted values and Lanzoni et al. (2007) suggest for the Blue straggle stars (BSS) of M55 an unusually high primordial population of binaries compared to other GGCs. So, according with previous studies and due to its age, $\sim$ 13.5 ± 1.0 Gyr (Dotter et al., 2010), $\sim$12.3 ± 1.7 Gyr (Salaris & Weiss, 2002), is a perfect candidate to study the chemical evolution and star formation history of the Milky Way and despite the extensive photometric (Kaluzny et al., 2010, Olech et al., 1999, Richter et al., 1999, Rozyczka et al., 2013) and kinematics and proper motion studies (Sariya et al., 2012, Zloczewski et al., 2011) of this cluster, there is a lack of spectroscopic studies in the last two decade. Carretta et al. (2009, 2010, 2009), Pilachowski et al. (1984) and recently Mucciarelli et al. (2017), Wang et al. (2017) measured a number of elements ranging from Oxygen to Europium by using high-resolution spectra. Compared with the previous works, our study will be the most accurate study of its chemical abundances in the past 20 years. Our work will be focus on revealing chemical abundance variations and how these could relate to the environment in which this cluster formed.

2.1.1 Characteristics of NGC 6809

Celestial coordinates are used to help locate objects on the sky. Table 2.1 summarized the most important coordinates systems. Equatorial coordinates: Right Ascension (RA) and Declination (Dec) from J2000 (locations of celestial objects in the year 2000) and Galactic coordinates: Galactic longitude (l) and Galactic latitude (b) from Goldsbury et al. (2010). In this table is also include the distance from NGC 6809 to the sun (R_{sun}) and the distance to the galactic center (R_{gc}) from Harris catalog (Harris, 2010). In table 2.2 the following properties of NGC 6809 are listed: A reddening value (E(B-V)) from Webbink (1985). The metallicity ([Fe/H]), distance modulus $(m\text{-}M)_V$, absolute magnitude (M_V) and the spectral type from Harris Catalogue (Harris, 2010). For the structural parameters: The core radius r_c and half light-radius r_h (radius enclosing half the total luminosity) from Trager et al. (1995). The age is from Salaris & Weiss (2002) , the mass from Boyles et al. (2011) and the heliocentric radial velocity from Harris Catalogue (Harris, 2010). All this characteristics and values are listed in Table 2.3.

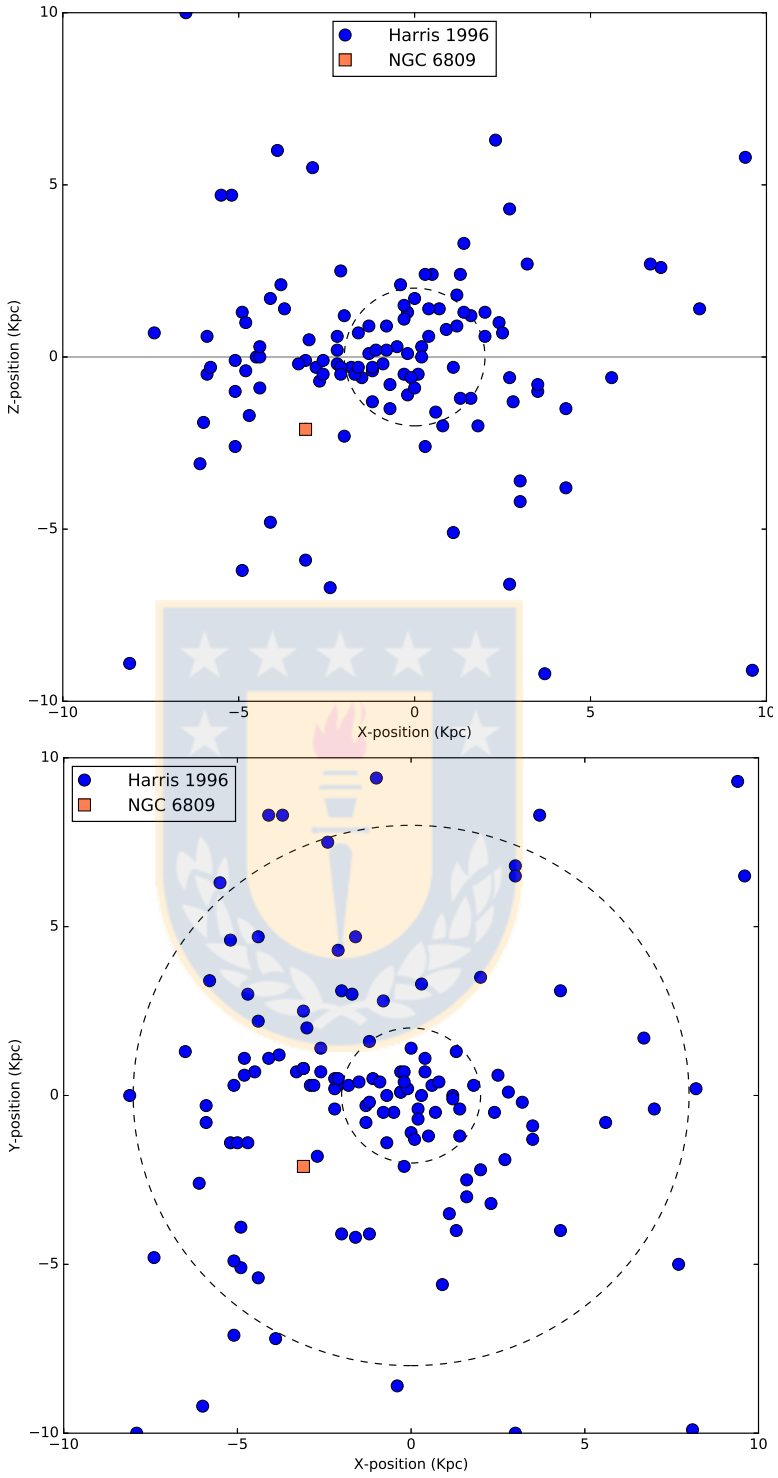

FIGURE 2.2: Position of NGC 6809 in the X-Z plane and the X-Y plane. Orange square represent NGC 6809 and blue filled circle represent the data from other Globular Clusters (GC's) from Harris (2010). Dashed lines are the distance from the Galactic Center to the Sun $R_{\odot}$= 8 kpc and the Bulge radius with R_{bulge}= 2 kpc and the black line is the Galactic plane. Source: self made.

Chapter 3

Method: Data Reduction and Techniques

3.1 Analysis Method

3.1.1 Observation data

Our dataset consists of high-resolution spectra collected at FLAMES@UVES spectrograph mounted on UT2 (Kueyen) at ESO-VLT Observatory in Cerro Paranal during June of 2014 (ESO program ID 093.D-0286(A)). Our sample includes 11 stars, which belong to the Giant Branch cluster sequence with infrared magnitude from Two Micron All-Sky Survey (2MASS) between K_s=7.97 and K_s=9.70. Figure 3.1 show the location of the members in the colour-magnitude diagram (CMD) of J-K colour versus K magnitude.

The spectral coverage is of $\sim$ 200nm (from 480 to 680nm), with the central wavelength at $\sim$ 580nm and with a mean resolution of R $\simeq$ 47000. We stacked several spectra in order to increment the signal-to-noise (S/N) see Figures 3.2, 3.3. The final S/N between 60 and 200 at 600nm (see Table 3.1)

3.1.2 Data reduction

Raw data were reduced using the dedicated pipeline[1]. Data reduction includes bias subtraction, flat-field correction, wavelength calibration and spectral rectification. We subtracted the sky using the *sarith* package and radial velocities were measured by the

[1] http://www.eso.org/sci/software/pipelines/

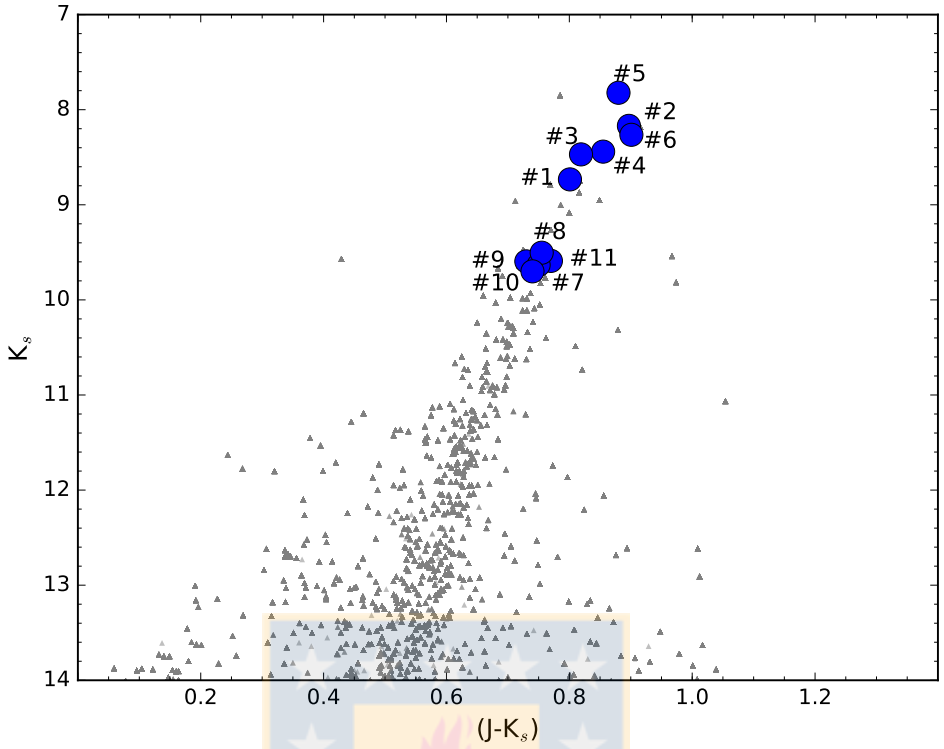

FIGURE 3.1: Colour-Magnitude diagram (CMD) of NGC 6809 from 2MASS photometry. Blue circles are our observed UVES sample. Source: self made.

fxcor package in IRAF [2]. This task cross-correlates the spectrum of the star with a template. Observed radial velocities were then corrected to the heliocentric system. NGC 6809 has a large heliocentric radial velocity RV_H. The mean value we obtained is:

$$\langle RV_H \rangle = 174.7 \pm 3.2 kms^{-1}$$

this value is in excellent agreement with the literature Harris (1996) gives $\langle RV_H \rangle = 174.7 \pm 0.3$ kms^{-1}, Pryor et al. (1991) found a value of $\langle RV_H \rangle = 176 \pm 0.9$km^{-1}, Lane et al. (2011) provide a mean value of $\langle RV_H \rangle = 178 \pm 1.21$ km^{-1} and finally Wang et al. (2017) found a radial velocity of $\langle RV_H \rangle = 173.6 \pm 3.7$ km^{-1} by using our targets. We considerer our value in agreement with the previous studies.

[2]IRAF is distributed by the National Optical Astronomy Observatory, which is operated by the Association of Universities for Research in Astronomy, Inc.., under cooperative agreement with the National Science Foundation

Star ID	RA [degrees]	Dec [degrees]	J [mag]	H [mag]	K [mag]	RV_H [Kms^{-1}]	T_{eff} [K]	log(g) [dex]	v_t [Kms^{-1}]	[Fe/H] [dex]	S/N @6000 [Å]
1	294.937416	-31.003833	9.53	8.88	8.73	180.34	4209	0.14	2.02	-2.21	165
2	294.974874	-30.960861	9.06	8.32	8.17	176.42	4105	0.28	1.86	-1.93	136
3	294.983416	-30.921388	9.28	8.66	8.47	171.12	4144	0.06	2.13	-1.97	159
4	294.998541	-30.919472	9.29	8.60	8.44	176.73	4162	0.51	1.76	-1.94	142
5	295.016999	-30.972416	8.70	7.97	7.82	170.25	4022	0.08	2.07	-1.93	114
6	295.033583	-30.971166	9.16	8.42	8.26	173.38	4119	0.30	1.80	-1.93	123
7	294.929999	-30.947777	10.38	9.77	9.63	171.69	4376	0.66	1.81	-2.05	145
8	294.960916	-30.928388	10.25	9.61	9.50	175.85	4293	0.54	1.72	-2.08	72
9	295.007583	-30.979166	10.32	9.68	9.59	174.19	4350	0.61	1.77	-2.04	158
10	295.009999	-30.785722	10.44	9.80	9.70	171.62	4387	0.63	1.75	-2.01	60
11	295.018124	-31.062777	10.36	9.71	9.59	180.25	4348	0.65	1.77	-2.06	200
Cluster						174.7				-2.01	
Error						3.26				0.02	

TABLE 3.1: Coordinates, 2MASS (J,H,K) magnitudes, heliocentric radial velocities, atmospheric parameters adopted and the typical S/N for the observed stars.

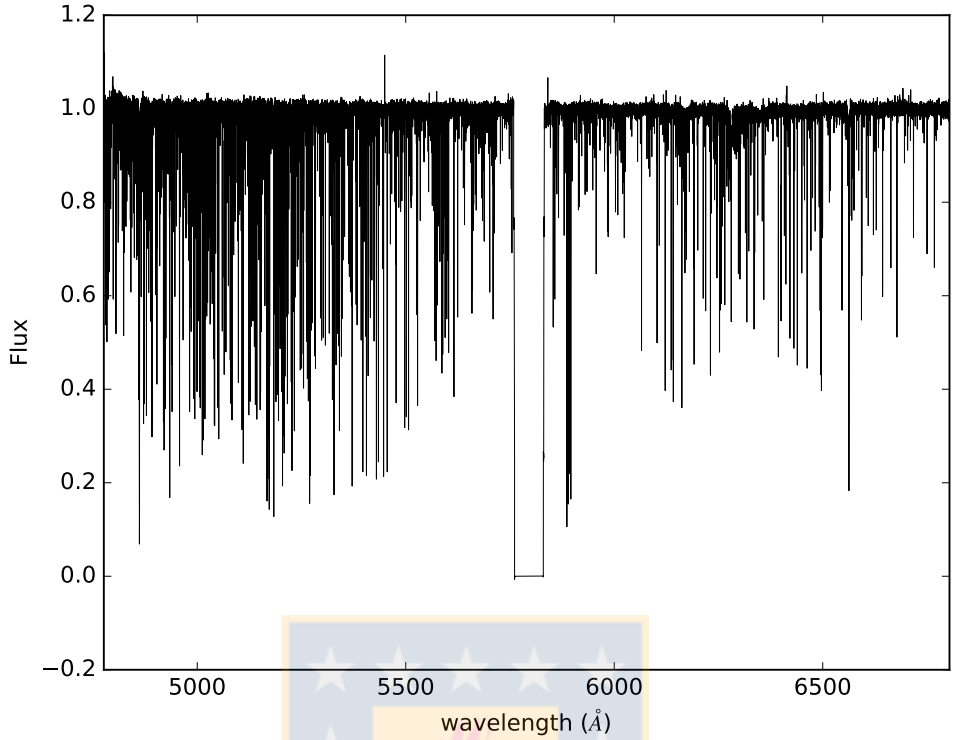

FIGURE 3.2: General view of our best UVES spectrum: star #9, covering a wavelength range between 4700Å to 6800Å is posible indentified a gap between 5760Å to 5840Å. Source: self made.

Table 3.1 lists the basic parameters of the observed stars: the ID, J2000 coordinates (RA and Dec in degrees), J, H, K_s magnitudes from 2MASS, heliocentric radial velocity RV_H [kms^{-1}], adopted atmospheric parameters (including [Fe/H]) and the typical S/N for each star. In addition, we report the cluster mean radial velocity and mean [Fe/H] abundance with their errors. The determination of the atmospheric parameters is discussed in the following section.

3.2 Atmospheric Parameters, Abundances and Error determination

3.2.1 Atmospheric parameters

A first estimation of stellar parameters was obtain by using infrared photometry from 2MASS and following the next procedure: effective temperature (T_{eff}) from all the stars was derived from the $(J-K)$ and $(J-H)$ colors using the relation of Alonso et al. (1999) with photometry from the Two Micron All-Sky Survey (2MASS)[3]. Equation (3.1), (3.2)

[3]http://www.ipac.caltech.edu/2mass/

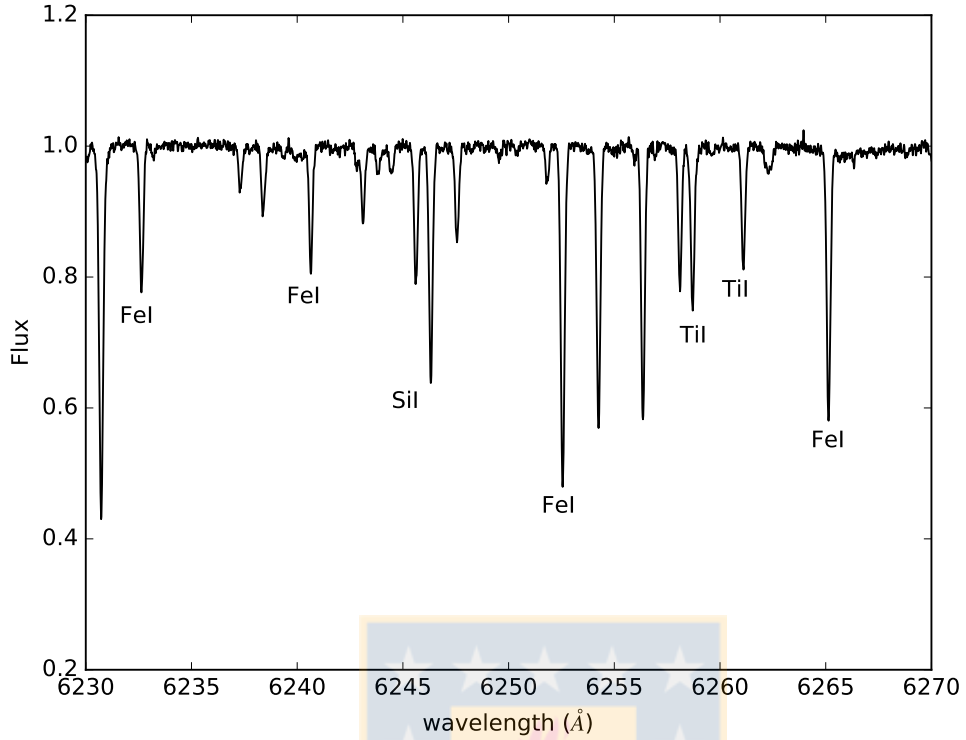

FIGURE 3.3: Detail view of our best UVES spectrum: Target 9, covering a wavelength range between 6230Å to 6270Å. Several important lineas of FeI, SiI and TiI are identified. Source: self made.

and (3.3) were used for this purpose.

$$T_{eff} = \frac{5040}{\theta_{eff}} \tag{3.1}$$

with

$$\begin{aligned} \theta_{eff} &= 0.5977 + 1.015(J-H) - 0.1020(J-H)^2 - 0.01029(J-H)[Fe/H] \cdots \\ &\quad \cdots + 0.03006[Fe/H] + 0.01012[Fe/H]^2 \end{aligned} \tag{3.2}$$

for the (J-H) color and

$$\theta_{eff} = 0.5816 + 0.9134(J-K) - 0.1443(J-K)^2 \tag{3.3}$$

for the (J-K) color. With a reddening value of E(J-H)= 0.25·E(B-V) and E(J-K)= 0.36·E(B-V), where E(B-V)= 0.08 and [Fe/H]=1.94 are from Harris (2010).

Surface gravities log(g) were obtained from the canonical equation:

$$log\left(\frac{g}{g_{\odot}}\right) = log\left(\frac{M}{M_{\odot}}\right) + 4log\left(\frac{T_{eff}}{T_{\odot}}\right) - log\left(\frac{L}{L_{\odot}}\right) \tag{3.4}$$

were the mass $M/M_{\odot}$ was assumed to be $0.8M_{\odot}$ and the luminosity $L/L_{\odot}$ was obtained from the absolute magnitude M_V assuming a distance modulus of (m-M)=13.89 from Harris (2010). The bolometric correction (BC) was derived by adopting the BC-T_{eff} relation of Buzzoni et al. (2010).

$$BC = -6.75 \cdot log\left(\frac{T_{eff}}{9500}\right) \tag{3.5}$$

Finally, microturbulence velocity (v_t) was obtained from the relation v_t - logg used in Gratton et al. (1999)

$$v_t = 2.22 - 0.322 \cdot log(g) \tag{3.6}$$

for the same type of stars as in our sample. This initial atmospheric parameters are only initial guesses. For this analysis, model atmosphere were calculated iteratively using ATLAS9 code (Kurucz, 1970) adopting the values of T_{eff}, v_t and log(g) determine in the Subsection 3.2.1 and using [Fe/H]=-1.94 dex value from Harris (1996). The program MOOG (Sneden, 1973) was used to determine the chemical abundances and the spectroscopic stellar parameters. MOOG is a FORTRAN code that performs a spectral lines analysis and spectrum synthesis assuming Local Thermodynamic Equilibrium (LTE). The [Fe/H] value of the model was changed at each iteration according to the output of the abundance analysis. Then, during the abundance analysis and in order to obtain the final stellar parameters we use three conditions to constrain T_{eff}, log(g) and v_t :

1. We impose excitation potential (EP) equilibrium of the FeI lines for T_{eff}.
2. We minimize any dependence on FeI abundances as a function of equivalent widths (EWs) for the v_t.
3. We impose that the average abundance derived from species ionised differenttly (in this case FeI and FeII lines) to be approximately equal for log(g).

The adopted atmospheric parameters are listed in table 3.1.

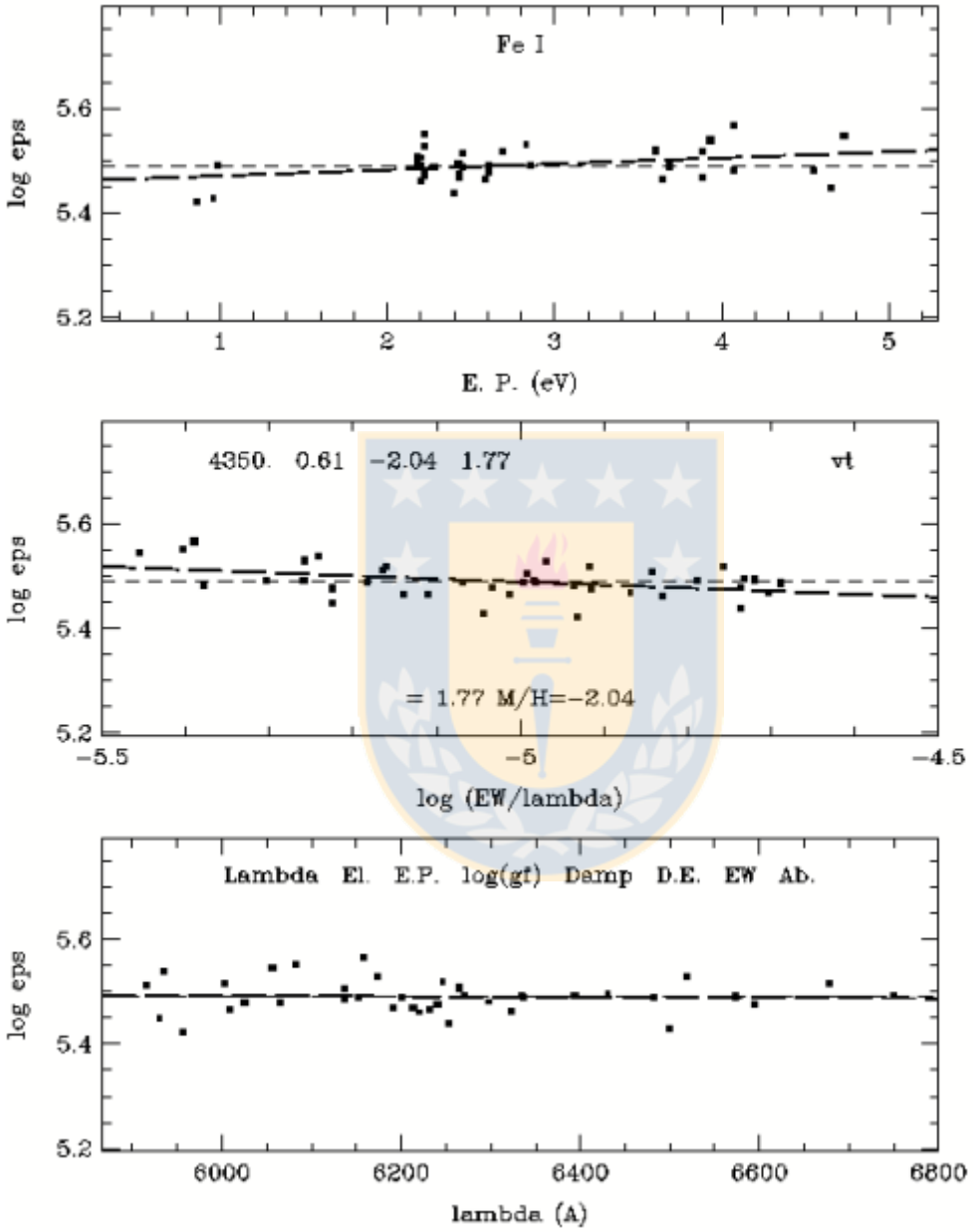

FIGURE 3.4: Output window of MOOG. Top plot represent the abundance versus E.P. Middle plot represent abundance versus EW. Bottom plot represent abundance versus wavelength. Dash lines shows the trend and the mean value.

3.2.2 Chemical abundances

In our study, we used two different methods to measure abundances: equivalent widths (EW's) and spectral synthesis. A detailed explanation of the method used to measure the EW's is given in Marino et al. (2008). For those elements whose lines are weak, affected by blending or hyperfine and isotopic splitting we used the spectrum-synthesis method. The line list for the chemical analysis is the one described in Villanova & Geisler (2011). Abundances for our targets were determined by an iterative process in which the synthetic spectrum is compared to the observed one modifying the abundance in each step until reaching the best-fit value as the one that minimises the rms scatter. For this purpose, five synthetic spectra were generated for each line with $\sim$ 0.20 dex abundance step.

The MOOG software requires a model atmosphere and the EW tables as input. The output is the average element abundance along with plots of abundance with E.P., reduced EW, and wavelength.

In this work we measured the light elements O, Na, Mg, Al: Both Oxygen and Sodium abundances were obtained using the spectral synthesis method. For O we used the forbidden [OI] line at 6300 Å, for Na abundances we used the Na I doublet at 5682 - 5688 Å. Non-LTE (NLTE) corrections were made for Na lines; this will be discussed in more detail in Subsection 4.1.4.1. Magnesium abundances are typically derived from three high excitation lines: 5711, 6318 and 6319 Å, however in our study Mg I abundances has been inferred from spectral synthesis only of the transitions at $\sim$ 5711.09 Å. Aluminum abundances are derived from the doublet at 6696 - 6698 Å.

Iron abundances were estimated through the EW's method using $\sim$ 38-51 lines for FeI and $\sim$ 5 lines for FeII. For Calcium, Titanium $\sim$ 5 and $\sim$ 15 lines respectively. Silicon abundances were inferred from several transitions within the spectral range 5645-61445 Å. SiI presents few features in the spectrum, so in this case, abundances derived from the EW's were cross-checked with the spectral synthesis method in order to obtain more accurate measurements.

By using spectral synthesis we determine abundances of the following iron peak elements: Sc (5684 Å) ,CuI (5218 Å), Co (5342 Å), VI (5670 Å), MnI (5420 Å), and ZnI (4811 Å). For Nickel and Chromium abundances we used a number of $\sim$ 17 - 23 and $\sim$ 8 isolated lines. NiI and CrI abundances are all derived by EW's method. Manganese, Cobalt and Cooper abundances are available only for ten stars.

Finally, to complete our analysis and include key heavy elements. the abundances of Y, Zr, La, Ce, Nd, Eu, Ba and Dy were obtained. For this set of elements only the spectrum-synthesis method was used. Even if several of these elements suffer hyperfine splitting only Ba lines, beeing strong, need this splitting to be taken into account. For Zr II we used the available lines at 5112 and 5350 Å. Zirconium, Dysprosium and Cerium abundances are available only for ten stars. A list of all the derived chemical abundances and the adopted solar abundances we used are reported in Table 4.1.

3.2.3 Errors

To estimate the internal errors associated with our spectroscopic atmospheric parameters we perform the following procedure.

For T_{eff} we calculated, in the relation between abundance versus potential excitation (E.P), the errors associated with the slopes by performing the best least square fit to each star. The average of the errors correspond to the typical error on the slope. Then we selected three stars representative of the entire sample star#10, star#4, and star#5 with high, intermediate and low T_{eff} respectively. For each of them, we fixed log(g), v_t and [Fe/H] and varied the temperature until the slope of the line that best fits the relation between abundances and E.P. given by MOOG became equal to the respective mean error we find. The difference in temperature, represents an estimate of the error in temperature itself. In order to associate an error to the measures of gravity we have varied the gravity of the three representative stars such that the relation [Fe/H]-$\langle\sigma_{star}[FeI/H]\rangle$ = [Fe/H]+$\langle\sigma_{star}[FeII/H]\rangle$ was satisfied for each. Where $\langle\sigma_{star}[Fe/H]\rangle$ is the dispersion given by MOOG for the corresponding lines, divided by the square of the number of lines minus one. (Marino et al., 2008). For v_t the same procedure as in temperature was applied, but in this case, using the relation between abundance and EWs. The error of the mean [Fe/H] what obtained by dividing the rms (σ_{obs}) by $\sqrt{N_{stars}-1}$.

We find ΔT_{eff}=40k, Δv_t=0.07 kms^{-1}, Δlog(g)= 0.10 and Δ[Fe/H]= 0.02 dex as our errors on the atmospheric parameters. Then we choose star #7 as representative of the sample, varied its T_{eff}, log(g), [Fe/H], and v_t according the atmospheric errors we just obtained, and redetermining the abundances.

Finally, we measured the error due to the noise in the spectra for each star. This error was obtained for elements whose abundance was obtained by EWs, as the errors on the mean given by MOOG. On the other hand, elements whose abundances was obtained by spectral synthesis the error is the output of the fitting procedure. The final errors (σ_{Tot}) in our measured abundances are given by the relation:

[X/Fe]	Δ T_{eff} +40k	Δv_t 0.06 kms^{-1}	Δlog(g) 0.10	Δ[Fe/H] 0.02 dex	S/N	σ_{Tot}	σ_{Obs}
Δ([O/Fe])	0.03	0.02	0.04	0.01	0.01	0.05	0.18
Δ([Na/Fe])	0.03	0.03	-0.01	0.01	0.02	0.04	0.20
Δ([Mg/Fe])	-0.02	-0.04	-0.05	0.03	0.01	0.05	0.10
Δ([Al/Fe])	0.06	0.04	0.03	0.00	0.01	0.07	0.34
Δ([Si/Fe])	0.02	0.01	0.01	0.01	0.02	0.03	0.05
Δ([Sc/Fe])	0.00	0.00	0.05	0.00	0.01	0.05	0.05
Δ([Mn/Fe])	0.02	0.05	0.05	-0.04	0.01	0.07	0.04
Δ([Cu/Fe])	0.05	0.04	0.02	-0.01	0.01	0.06	0.07
Δ([Zn/Fe])	-0.03	0.02	0.03	0.02	0.04	0.06	0.09
Δ([Ba/Fe])	0.04	-0.03	0.03	0.04	0.03	0.07	0.11
Δ([Ce/Fe])	0.04	0.01	0.02	0.02	0.01	0.05	0.06
Δ([Co/Fe])	0.06	0.03	-0.01	0.01	0.01	0.06	0.06
Δ([Dy/Fe])	0.04	0.03	0.05	-0.02	0.01	0.07	0.09
Δ(Eu/Fe])	0.01	-0.02	0.03	0.04	0.03	0.06	0.07
Δ([Y/Fe])	0.05	0.04	0.05	-0.02	0.03	0.08	0.13
Δ([La/Fe])	0.03	0.02	0.03	0.02	0.01	0.05	0.06
Δ([Nd/Fe])	0.02	0.00	0.04	0.01	0.02	0.04	0.06
Δ([V/Fe])	0.07	0.02	-0.01	0.04	0.02	0.07	0.06
Δ([Ca/Fe])	0.06	-0.01	0.00	0.02	0.10	0.11	0.05
Δ([TiI/Fe])	0.08	0.01	0.00	0.01	0.02	0.08	0.04
Δ([TiII/Fe])	0.01	0.01	0.04	0.00	0.04	0.05	0.09
Δ([Cr/Fe])	0.06	0.01	0.00	0.01	0.05	0.07	0.05
Δ([Ni/Fe])	0.07	0.01	0.00	0.01	0.02	0.07	0.02
Δ([Zr/Fe])	-0.03	-0.03	0.03	0.02	0.01	0.06	0.07
Δ([Fe/H])	-0.01	-0.01	-0.01	-0.01	-0.01	0.02	0.08

TABLE 3.2: Estimated errors on [X/Fe] due to the stellar parameters (columns 2 to 5) and to spectral noise (column 6) for star #7. Column 7 is the total internal uncertainty calculated as the root square of the sum of the squared of columns 2 to 6. Column 8 is the observed dispersion.

$$\sigma_{tot} = \sqrt{\sigma^2_{T_{eff}} + \sigma^2_{log(g)} + \sigma^2_{v_t} + \sigma^2 + \sigma^2_{[Fe/H]} + \sigma^2_{S/N}} \tag{3.7}$$

The resulting errors for each [X/Fe] ratio, including the observed dispersion (σ_{Obs}) and the error of the S/N are report in Table 3.2.

Chapter 4

Results

4.1 Abundances Results

It has been realized that element abundances and especially their ratios represent a very important source of information since they allow us to impose constraints on both stellar nucleosynthesis and galaxy formation mechanisms. In particular, the study of the abundances of single elements was made possible also by the increasing development in both the observational and theoretical studies of supernovae (SNe). A large body of evidence now shows that the stars in a GC do not share the same chemical composition (Gratton et al., 2012). As a general rule we can define a globular cluster as an object that is homogeneous in its Fe content and most other heavy elements, but the light elements Li, C, N, O, Na, Mg and Al can show substantial intracluster variations. Advances in instrumentation and spectrum analysis methods in the past 20 years made it possible to compute stellar abundances accurately with an error of only about 10%. This revealed interesting regularities in the abundance variations between stars of different stellar populations. For instance, regularities for alpha-elements (e.g. O, Mg, Ca) or those of the iron peak ($22< Z < 28$, i.e. Ti, V, Cr, Mn, Fe, Co, Ni) indicate that the chemical and dynamical evolution of the Galaxy is, in fact, very complex. Various substructures of the Milky Way (disk, bulge, halo, globular clusters) formed on different timescales and by different mechanisms. Our work involves the most accurate measurement of abundances carried out in NGC 6809. Our aim is to study the chemical evolution of NGC 6809 and also looking for possible MPs. In the following sections, we present chemical abundances for α, Fe-peak, light and heavy elements. We compare our results with Halo and Disc field stars as well Galactic Globular Clusters that have NGC 6809's metallicity.

[X/Fe]	1	2	3	4	5	6	7	8	9	10	11	⟨[X/Fe]⟩	Sun
[O/Fe]	+0.43	+0.08	+0.38	+0.09	+0.21	+0.13	-0.17	+0.13	-0.02	-0.19	+0.18	+0.11±0.05	8.83
[Na/Fe]	+0.05	+0.53	-0.06	+0.52	+0.25	+0.42	+0.53	+0.46	+0.44	+0.33	+0.36	+0.33±0.06	6.32
[Mg/Fe]	+0.48	+0.51	+0.55	+0.24	+0.31	+0.45	+0.27	+0.53	+0.41	+0.39	+0.45	+0.41±0.03	7.56
[Al/Fe]	+0.32	+0.95	+0.16	+1.01	+0.82	+1.00	+1.24	+0.79	+1.18	+1.32	+0.72	+0.86±0.10	6.43
[Si/Fe]	+0.50	+0.50	+0.59	+0.39	+0.48	+0.53	+0.49	+0.54	+0.59	+0.45	+0.48	+0.50±0.01	7.61
[Ca/Fe]	+0.40	+0.31	+0.39	+0.30	+0.33	+0.30	+0.37	+0.36	+0.36	+0.28	+0.36	+0.34±0.01	6.39
[Sc/Fe]	+0.19	+0.18	+0.14	+0.13	+0.21	+0.21	+0.08	+0.08	+0.10	+0.06	+0.12	+0.13±0.01	3.12
[Ti/Fe]	+0.37	+0.33	+0.36	+0.41	+0.38	+0.49	+0.37	+0.33	+0.34	+0.24	+0.34	+0.36±0.02	4.92
[V/Fe]	+0.08	+0.10	+0.09	+0.10	+0.14	+0.14	+0.15	-0.02	+0.06	+0.19	+0.16	+0.10±0.01	4.00
[Cr/Fe]	-0.01	-0.03	-0.10	-0.01	+0.10	0.00	-0.01	+0.04	+0.02	-0.08	+0.03	0.00±0.01	5.63
[Mn/Fe]	-0.29	-0.25	-0.28	-0.24	-0.21	0.24	-0.39	-0.30	-0.33	.....	-0.29	-0.28±0.01	5.37
[Co/Fe]	+0.32	+0.12	+0.20	+0.10	+0.12	+0.10	+0.19	+0.19	+0.17	.....	+0.24	+0.17±0.01	4.93
[Ni/Fe]	+0.01	-0.04	-0.03	-0.02	-0.03	-0.02	+0.01	+0.01	+0.04	-0.02	+0.01	0.00±0.01	6.26
[Cu/Fe]	-0.13	-0.28	-0.29	-0.32	-0.40	-0.37	-0.19	-0.27	0.22	.....	-0.34	-0.28±0.02	4.19
[Zn/Fe]	+0.36	+0.23	+0.27	+0.16	+0.33	+0.28	+0.09	+0.25	+0.11	+0.07	+0.16	+0.22±0.02	4.61
[Y/Fe]	+0.24	+0.12	-0.02	+0.10	+0.13	+0.07	-0.07	-0.02	-0.08	-0.12	-0.08	+0.02±0.04	2.25
[Zr/Fe]	+0.39	+0.13	+0.24	+0.31	+0.26	+0.19	+0.17	+0.25	+0.15	.....	+0.22	+0.23±0.02	2.56
[Ba/Fe]	+0.03	-0.09	+0.13	-0.03	+0.05	-0.07	-0.18	-0.19	-0.21	-0.15	-0.21	-0.08±0.03	2.34
[La/Fe]	+0.35	+0.24	+0.18	+0.27	+0.29	+0.25	+0.23	+0.17	+0.16	+0.11	+0.19	+0.22±0.01	1.26
[Ce/Fe]	-0.05	-0.08	-0.17	-0.11	+0.07	-0.07	-0.06	-0.11	-0.18	.....	-0.14	-0.09±0.01	1.53
[Nd/Fe]	+0.40	+0.31	+0.26	+0.36	+0.43	+0.39	+0.30	+0.25	+0.25	+0.22	+0.30	+0.31±0.01	1.59
[Eu/Fe]	+0.64	+0.54	+0.47	+0.63	+0.59	+0.63	+0.42	+0.54	+0.57	+0.41	+0.56	+0.54±0.02	0.52
[Dy/Fe]	+0.30	+0.13	+0.05	+0.17	+0.17	+0.25	+0.25	+0.15	+0.16	.....	-0.06	+0.15±0.02	1.10
[α/Fe]	+0.43	+0.41	+0.47	+0.33	+0.37	+0.44	+0.37	+0.44	+0.42	+0.34	+0.40	+0.40±0.01	

TABLE 4.1: [X/Fe] for individual stars (columns 2 to 12) and the mean abundance ratios for the cluster (column 13). The abundances for Ti is the mean of those obtain from the neutral (TiI) and singly ionized species (TiII). The errors are statistical errors obtained of the mean. For Na abundances the NLTE values are report.

4.1.1 Alpha elements

A common feature in almost all the Globular Cluster and Halo field stars as well in metal-poor stars in the Milky Way, is an over-abundance in the α elements content.To date the only exception found among GCs is Rup. 106 (Villanova et al., 2013) which shows solar α elements abundances in spite having [Fe/H]=-1.5 dex. The enhancement of alpha elements in the halo has been confirmed by numerous studies, both in the field and the globular cluster system (Barbuy et al., 1985, Gratton & Sneden, 1988, 1991, McWilliam et al., 1995, Nissen et al., 1994). Figure 4.1 shows the [α/Fe] ratio as a function of the metallicity for each star in our sample, Galactic Globular Clusters (GGCs), Disc and Halo stars. In Figure 4.2 we plot the individual [Mg/Fe], [Si/Fe], [Ca/Fe] and [Ti/Fe] ratios as a function of the metallicity. Error bars were plotted in each panel. NGC 6809 follows the same trend as GGCs (e.g. NGC 5897, NGC 6426, NGC 4372 and NGC 4833) and is fully compatible with Halo field stars. The mean α content for each star is report in Table 4.1.

The α elements (O, Mg, Si, Ca, Ti) in our work are overabundant compared to the Sun. Since O shows a star to star variation it will be treated separately in the Subsection 4.1.4.1. Based only on Mg, Si, Ca and Ti we derived a mean α content of

$$\langle [\alpha/Fe] \rangle = +0.40 \pm 0.04$$

where the reported error is the error of the mean, the combined variation of Magnesium, Silicon, Calcium and Titanium should give us a better understanding of the data as it will reduce the scatter in them. As mentioned previously, the number of spectroscopic studies performed in NGC 6809 are really few. Comparing our results with previous studies perform in NGC 6809 we find

4.1.1.1 Magnesium

MgI abundances varies from 0.24<[Mg/Fe]<0.55 in our sample. The mean Magnesium content we found 0.41±0.03 dex. Mg values in this work are 0.06 dex lower than those found by Carretta et al. (2009).

4.1.1.2 Silicon

SiI abundances varies from [Si/Fe] = +0.39 to +0.59 dex. The average value we found $\langle$[Si/Fe]$\rangle$ = 0.50 ±0.01 (error of the mean). This value is 0.12 dex higher than the value

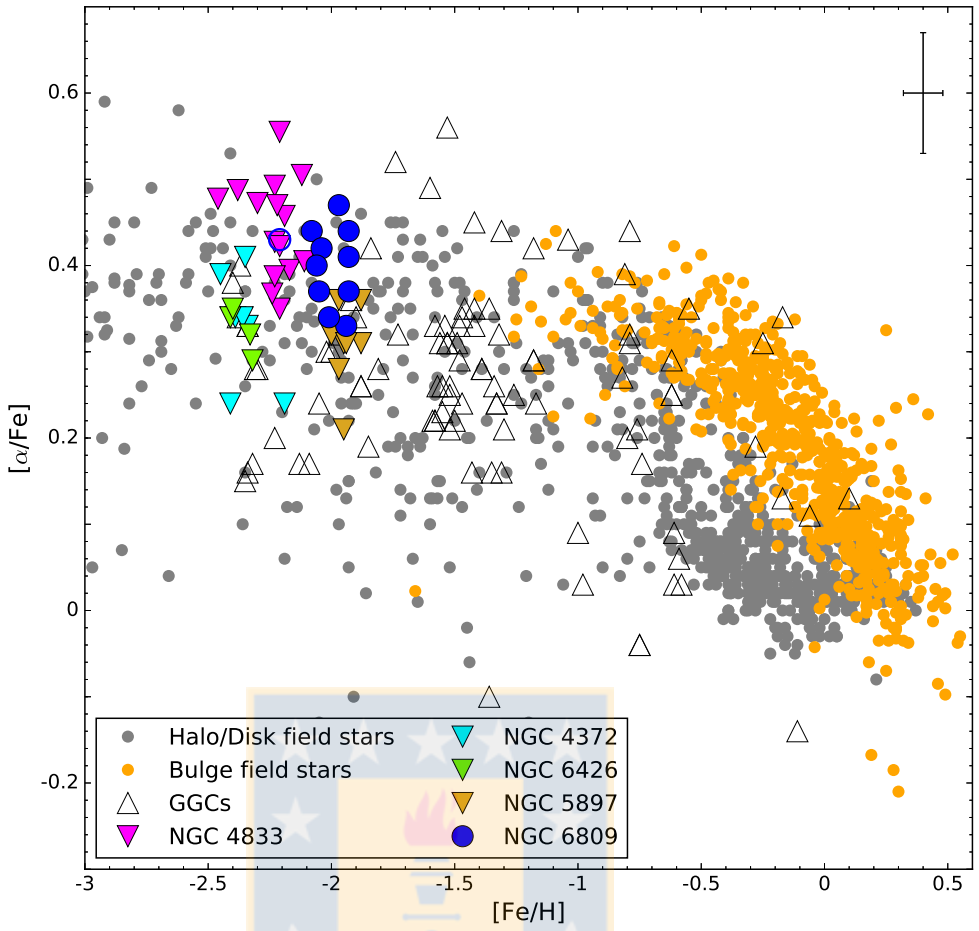

FIGURE 4.1: [α/Fe] ratio versus [Fe/H]. Filled blue circles are our data for NGC 6809. Open blue circle is our data for star #1 (the most metal poor of our sample). Triangles represent different GCs samples: Empty black triangles: Galactic Globular cluster (Pritzl et al., 2005). Filled green triangles: NGC 6426 (Hanke et al., 2017). Filled cyan triangles: NGC 4372 (Valenzuela-Calderon et al. in prep). Filled magenta triangles: NGC 4833 (Roederer & Thompson, 2015).Filled golden triangles: NGC 5897 (Koch & McWilliam, 2014). Filled orange circles: Bulge field stars (Gonzalez et al., 2011). Filled gray circles: Halo and field stars (Cayrel et al., 2004, Venn et al., 2004). Source: self made.

report by Carretta et al. (2009) and 0.06 dex lower than Pilachowski et al. (1984) ver cuentas ineas usaron yo solo use 6

4.1.1.3 Calcium

CaI abundances varies from [Ca/Fe]= +0.28 to +0.40 dex. The cluster average is [Ca/Fe] = +0.34 ± 0.01 (error of the mean). Our mean Ca content is 0.04 dex higher than the mean found in Pilachowski et al. (1984) and 0.02 dex lower than the average value of Carretta et al. (2010).

4.1.1.4 Titanium

For this element we were able to measure the abundance of the ionised species (TiII). The average value found in this study is [TiI+TiII/Fe]= +0.36 ± 0.02 dex our results for NGC 6809 are 0.14 dex higher than those found in Pilachowski et al. (1984). Titanium values varies from +0.24 <[Ti/Fe]< 0.49. Although ionization equilibrium condition imposed while determining the stellar parameters should give us the same titanium abundance we see an average difference of 0.19 dex, the highest difference between TiI and TiII is found in stars #4, #1 and #6 respectively, with a difference of 0.30, 0.32 and 0.44 respectively. If we don't considered this stars, we found an average difference of 0.10 dex which is an acceptable value.

Additionally, for the pure α elements we found a mean value of [(Si+Ca)/Fe]= +0.41 this value is consistent with the mean value report above. The explanation of the α-enhancement observed in NGC 6809 is the classical SNII pollution of the proto-cluster cloud stars. This type of supernovae are relatively efficient producers of α-elements (Sneden, 2004). Analyzing both the total observational error and the observed scatter for Si, Ca and Ti (see Table 3.2), we conclude that there is no evidence of internal dispersion for these elements (dispersion in Mg will be treated separately in Subsection 4.1.4.2).

4.1.2 Iron and iron-peak Elements

The mean [Fe/H] value we found for this cluster is:

$$\langle [Fe/H] \rangle = -2.01 \pm 0.06$$

where the reported error is the error of the mean. We did not find signs of intrinsic spread since the dispersion in iron values are within the errors (see Tab. 3.2). We mark star #1 with a blue open circle in all the plots because this star have a difference of -0.2 dex compared to the average iron content and we will check for any other particularity. Excluding star #1 our mean iron content is [Fe/H]=-1.99∼0.01

Unlike α-elements, it is easy to find spectroscopic measurements of metallicity for NGC 6809 stars. Minniti et al. (1993) found a value of [Fe/H]=-1.95 dex by using only 2 stars, Carretta et al. (2009) found from 14 stars observed with UVES a value of [Fe/H]=-1.93±0.07 and recently Wang et al. (2017) who selected the targets we analyze in this paper found a value of [Fe/H]=-1.86 dex using UVES and GIRAFFE data (∼100 stars).

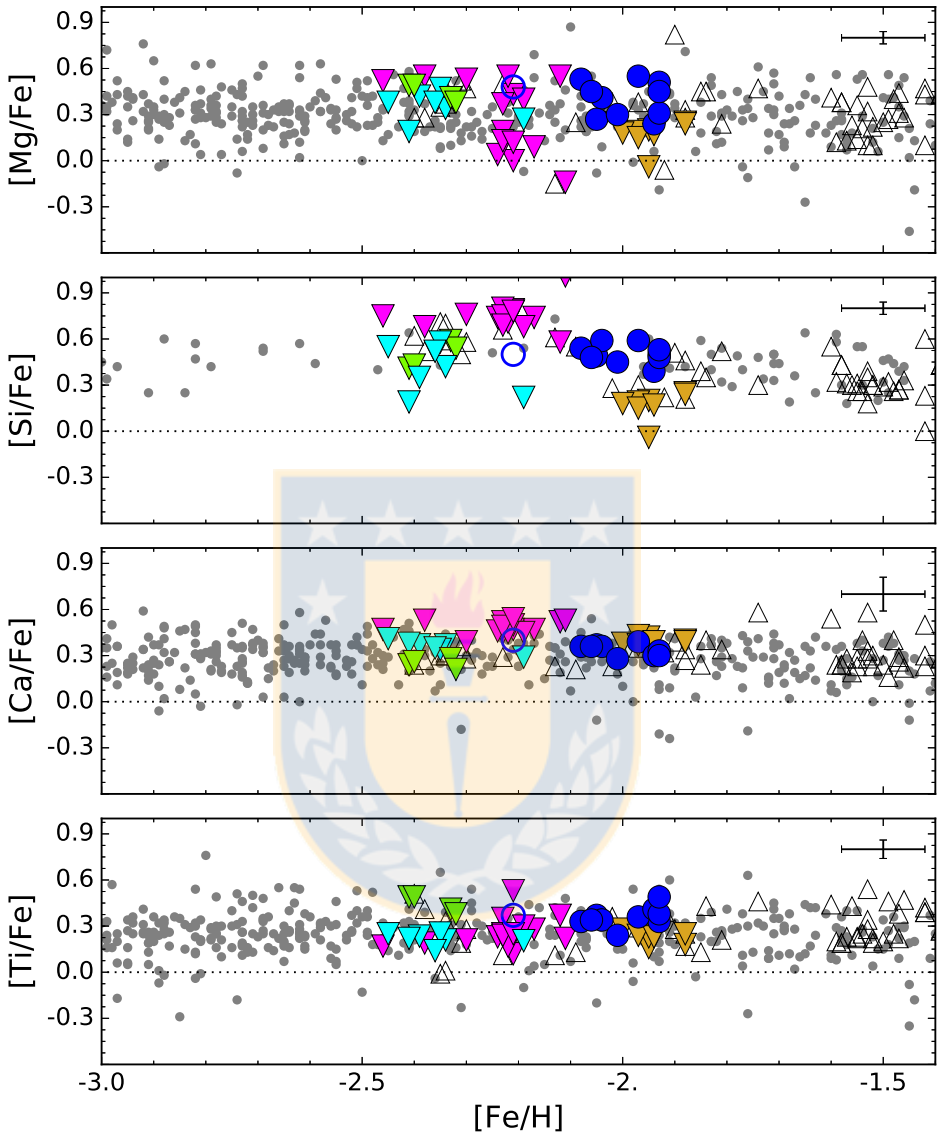

FIGURE 4.2: [Mg/Fe], [Si/Fe], [Ca/Fe] and [Ti/Fe] ratios versus [Fe/H]. Filled blue circles are our data for NGC 6809. Open blue circle is our data for star #1 (the most metal poor of our sample). Triangles represent different GCs samples: Empty black triangles: Galactic Globular cluster (Pritzl et al., 2005). Filled green triangles: NGC 6426 (Hanke et al., 2017). Filled cyan triangles: NGC 4372 (Valenzuela-Calderon et al. in prep). Filled magenta triangles: NGC 4833 (Roederer & Thompson, 2015).Filled golden triangles: NGC 5897 (Koch & McWilliam, 2014). Filled gray circles: Halo and field stars (Barklem et al., 2005, Cayrel et al., 2004, Venn et al., 2004). Source: self made.

Wang et al. (2017) measured iron abundances by using the same technique than us: equivalent width of both FeI and FeII unblended lines and the NLTE program MOOG. The difference in iron content between Wang et al. (2017) and our study is about 0.1 dex. There are two main difference between our work and Wang et al. (2017) that probably introduced this off-set. They applied non-LTE corrections(0.07 dex for the RGB sample and 0.10 dex for the AGB sample) to all the FeI lines and most of the sample in their work is conformed of GIRAFFE spectra that have lower resolution.

We find that [V/Fe], [Cr/Fe] and [Ni/Fe] ratios are ∼0 dex, whereas the [Cu/Fe] and [Mn/Fe] ratios are very low ∼-0.28 dex. [Sc/Fe], [Co/Fe] and [Zn/Fe] ratios are slightly overabundant ∼0.15 - 0.20 dex compared to solar values. Figure 4.3 shows our results for the iron-peak element Sc, Cr, Co, Cu, V, Mn, Ni, and Zn compared with Halo and Disc stars from the literature and different GC with similar metallicity to NGC 6809. Error bars were plotted in each panel.

4.1.2.1 Scandium

Several author has been discussed if Scandium follows Fe, that is [Sc/Fe]∼0 at all metallicities (Gratton & Sneden, 1991, McWilliam et al., 1995, Prochaska & McWilliam, 2000) or if Sc behaves like an α-element, that is [Sc/Fe]∼+0.2 in metal-poor Halo and thick-Disc stars (Battistini & Bensby, 2015, Zhao & Magain, 1990). Our results lie between both (see Fig.4.3) so, is not possible for us support any of this two possibilities. Additionally Koch & McWilliam (2014) and Marino et al. (2015) found for NGC 5897 and NGC 5286 means values of [Sc/Fe]=+0.08 and [Sc/Fe][1]=+0.09 respectively, values that are in agreement with our results in 1σ. Our Sc content is in completely agreement with the previous study perform in this cluster by Pilachowski et al. (1984).

4.1.2.2 Vanadium

Vanadium abundances varies from [V/Fe]= -0.02 to 0.19 dex. Good agreement was found between our abundances and those found in other GGCs. Vanadium abundances are generally solar scaled, our values closely follow Fe abundances. Pilachowski et al. (1984) found a mean V content of ∼ -0.20 dex, almost 0.30 dex lower than our result. This difference can be attributed to the number of VI lines used by them and the lower number of stars in which they could measure these abundances.

[1]We present [Sc/Fe] ratio only of UVES sample

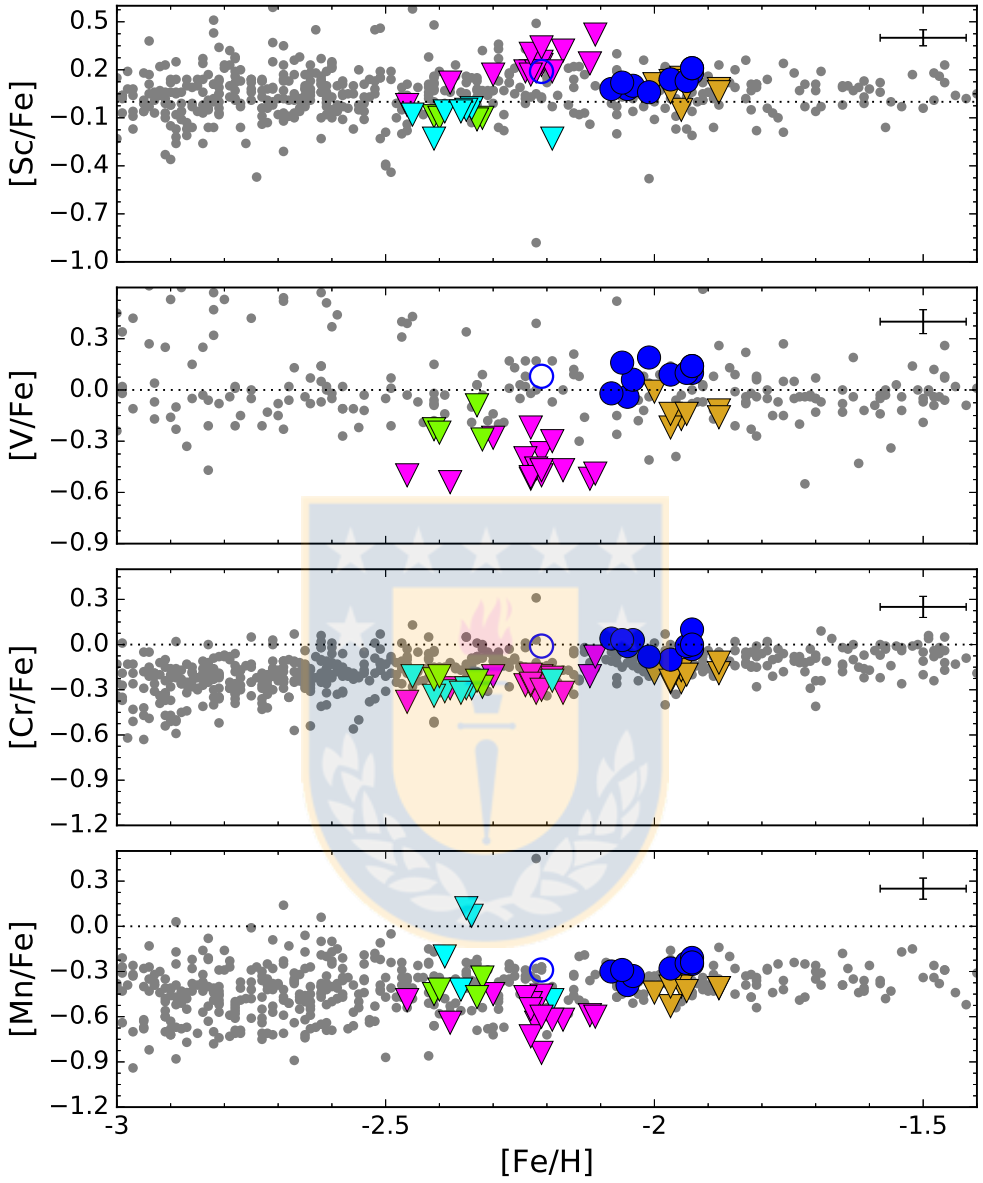

FIGURE 4.3: [Sc/Fe], [V/Fe], [Cr/Fe] and [Mn/Fe] ratios versus [Fe/H]. Filled blue circle are our data for NGC 6809. Open blue circle is our data for star #1 (the most metal poor of our sample). Triangles represent different GCs samples: Filled green triangles: NGC 6426 (Hanke et al., 2017). Filled cyan triangles: NGC 4372 (Valenzuela-Calderon et al. in prep). Filled magenta triangles: NGC 4833 (Roederer & Thompson, 2015). Filled golden triangles: NGC 5897 (Koch & McWilliam, 2014). Filled gray circles: Halo and Disc field stars (Barklem et al., 2005, Cayrel et al., 2004, Fulbright, 2000, Ishigaki et al., 2013, Roederer et al., 2014). Source: self made.

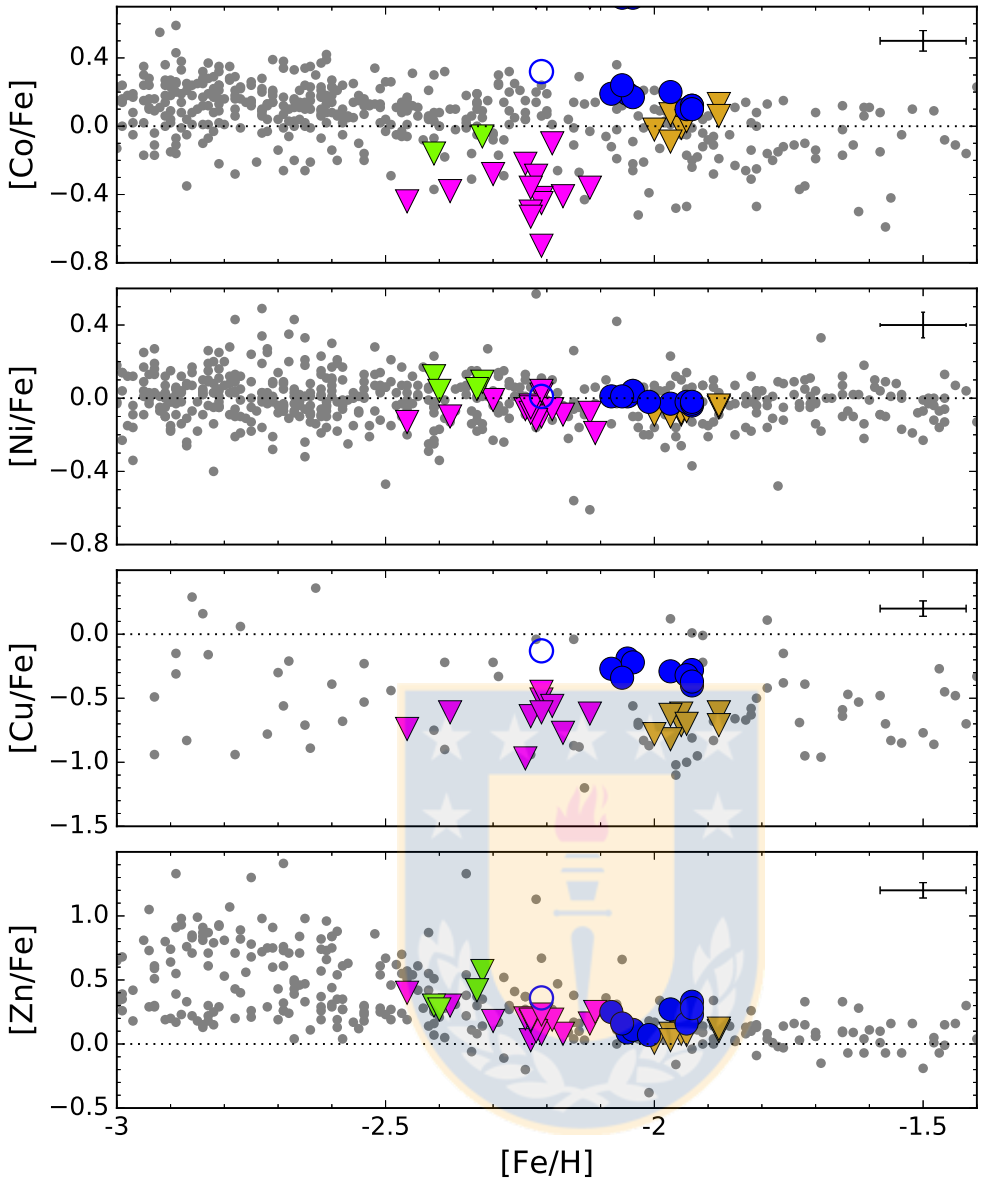

FIGURE 4.4: [Cu/Fe], [Ni/Fe], [Co/Fe] and [Zn/Fe] ratios versus [Fe/H]. Filled blue circle are our data for NGC 6809.Open blue circle is our data for star #1 (the most metal poor of our sample). Triangles represent different GCs samples: Filled green triangles: NGC 6426 (Hanke et al., 2017). Filled cyan triangles: NGC 4372 (Valenzuela-Calderon et al. in prep). Filled magenta triangles: NGC 4833 (Roederer & Thompson, 2015). Filled golden triangles: NGC 5897 (Koch & McWilliam, 2014). Filled gray circles: Halo and Disc field stars (Barklem et al., 2005, Cayrel et al., 2004, Fulbright, 2000, Ishigaki et al., 2013, Roederer et al., 2014). Source: self made.

4.1.2.3 Chromium

For Chromium ratios, stars follow a solar-scaled trend over the entire metallicity range with a large spread for [Fe/H]<-2. Our cluster with [Cr/Fe]=0.0, agrees with this trend. Our results are 0.35 dex lower than those found in Pilachowski et al. (1984), as in the case of Vanadium we strongly believe this difference could be since they measure Cr on average in only $\sim$ 5 lines.

4.1.2.4 Manganese

Sobeck et al. (2006) found for a sample of 19 GCs in the metallicity range -2.7<[Fe/H]<-0.7 that the Mn abundances in GC stars are equivalent to those of Halo field stars. They found that metallicity range a mean value of [Mn/Fe]=-0.37 dex for Globular Cluster stars and [Mn/Fe]=-0.36 for Halo field stars and despite our values for Mn are slightly higher than those found for other GC, our Mn content is in agreement with those found for NGC 4833 (Roederer & Thompson, 2015) (Carretta et al., 2014) and NGC 6426 (Hanke et al., 2017). Our mean Mn content is 0.15 lower than the value found in Pilachowski et al. (1984).

4.1.2.5 Cobalt

The chemical evolution of Co is thought to follow the same trend with metallicity as Cr, which is that Co evolves with Fe and [Co/Fe] remains constant. Observations show, however, that Co behaves like a α-element in the sense that it is enhanced at low metallicities by more or less $\sim$+0.2 dex, decreasing towards solar values at higher metallicities (Battistini & Bensby, 2015, Cayrel et al., 2004, Ishigaki et al., 2013). So, Co abundances in our sample are in accordance with Co trend for Halo field stars.

4.1.2.6 Nickel

Nickel abundances varies from [Ni/Fe]= -0.04 to 0.04 dex. [Ni/Fe] $\sim$ 0 over the entire Galactic metallicity range (Gratton et al., 2004). The star-to-star scatter in [Ni/Fe] increases with decreasing [Fe/H]. However no significant differences have been found between [Ni/Fe] in field stars, GCs. Our Ni values are in completely agreement with the galactic trend (see 4.4). Pilachowski et al. (1984) found a mean Ni content 0.14 dex lower than the value find in this work.

4.1.2.7 Cooper

As in the case of low-metallicity GCs (Simmerer et al., 2003), Copper is underabundant in NGC 6809. Koch & McWilliam (2014) give a value of [Cu/Fe]=-0.70 dex for NGC 5897 and Roederer & Thompson (2015) found a value of [Cu/Fe]= -0.65 dex for NGC 4833, Cu abundance ratio in our study is moderately higher than for both GCs. In general, for Cooper, stars follow a solar-scaled trend down to [Fe/H]$\sim$-0.9, below that metallicity as in the case of NGC 6809 they drop to [Cu/Fe]$\sim$-0.4. For Cu, if we considered the errors our results are in agreement with the literature.

4.1.2.8 Zinc

Observations of Halo stars perform for Bensby et al. (2005), Nissen et al. (2007) show that [Zn/Fe] is close to zero for metallicities in the interval -2.0 <[Fe/H]< +0.4 and in the range of -2.7 <[Fe/H]< -2 all [Zn/Fe] values are, however, positive with an average value of [Zn/Fe] $\sim$ +0.1. Despite our mean result for Zinc is +0.12 dex higher than the mean average, is compatible with the galactic trend.

Finally, analysing both the total observational error and the observed scatter for all the Fe-elements (see Table 3.2) we conclude that there is no evidence of internal dispersion for any of these elements.

4.1.3 Heavy Elements

We measured a number of elements with Z > 30: Y, Zr, Ba, La, Ce, Nd, Eu and Dy. In Figure 4.5 we plot [Y/Fe], [Ba/Fe], [La/Fe] and [Eu/Fe] as a function of [Fe/H], together with GGCs around NGC 6809 metallicity, Halo and Disc field stars.

4.1.3.1 Yttrium

For Yttrium, we found a mean value closed to $\sim$ 0.0. Galactic Globular Clusters follow this trend. The dispersion for Y is the highest among the n-capture elements (σ_{Obs} = 0.13 dex) measured here. However this dispersion is comparable to what is found in other studies at the same metallicity (James et al., 2004, Koch & McWilliam, 2014, Pritzl et al., 2005).

4.1.3.2 Zirconium

Mean Dysprosium abundance is enhanced by +0.35 dex and varies from [Nd/Fe]= +0.13 to +0.39 dex. Our mean Zr content show the large discrepancy with the study of Pilachowski et al. (1984), they found a mean [Zr/Fe] = -0.35 dex which is 0.70 dex lower than our results, we believe the main reason of this offset is since they only used one line available at 4613.92 Å, in four stars, compared with our ZrII abundances which are available for 10/11 stars.

4.1.3.3 Barium

Barium is mainly processed by s-process. [Ba/Fe] ratios in our work have slightly under-solar values. As in the case of Y, the dispersion for Ba abundances is 0.11 dex, nevertheless this dispersion not exceeded significantly the errors. Ivans et al. (2001), Lee & Carney (2002) found that Barium show a large dispersion at low metallicities, they also found [Ba/Fe] ratios for giant stars between -0.30 < [Ba/Fe] < +0.60 in GCs with -2.40 < [Fe/H] < -0.68. In this context our finding are fully compatible with these values (James et al., 2004).

4.1.3.4 Lanthanum

Lanthanum abundances in our sample have slightly over-abundant ($\sim$ +0.20 dex) values. Although literature values of La abundances are sparse for metal-poor stars, is well know that [La/Fe] ratio decrease with the metallicity for Halo field stars (Ishigaki et al., 2013).

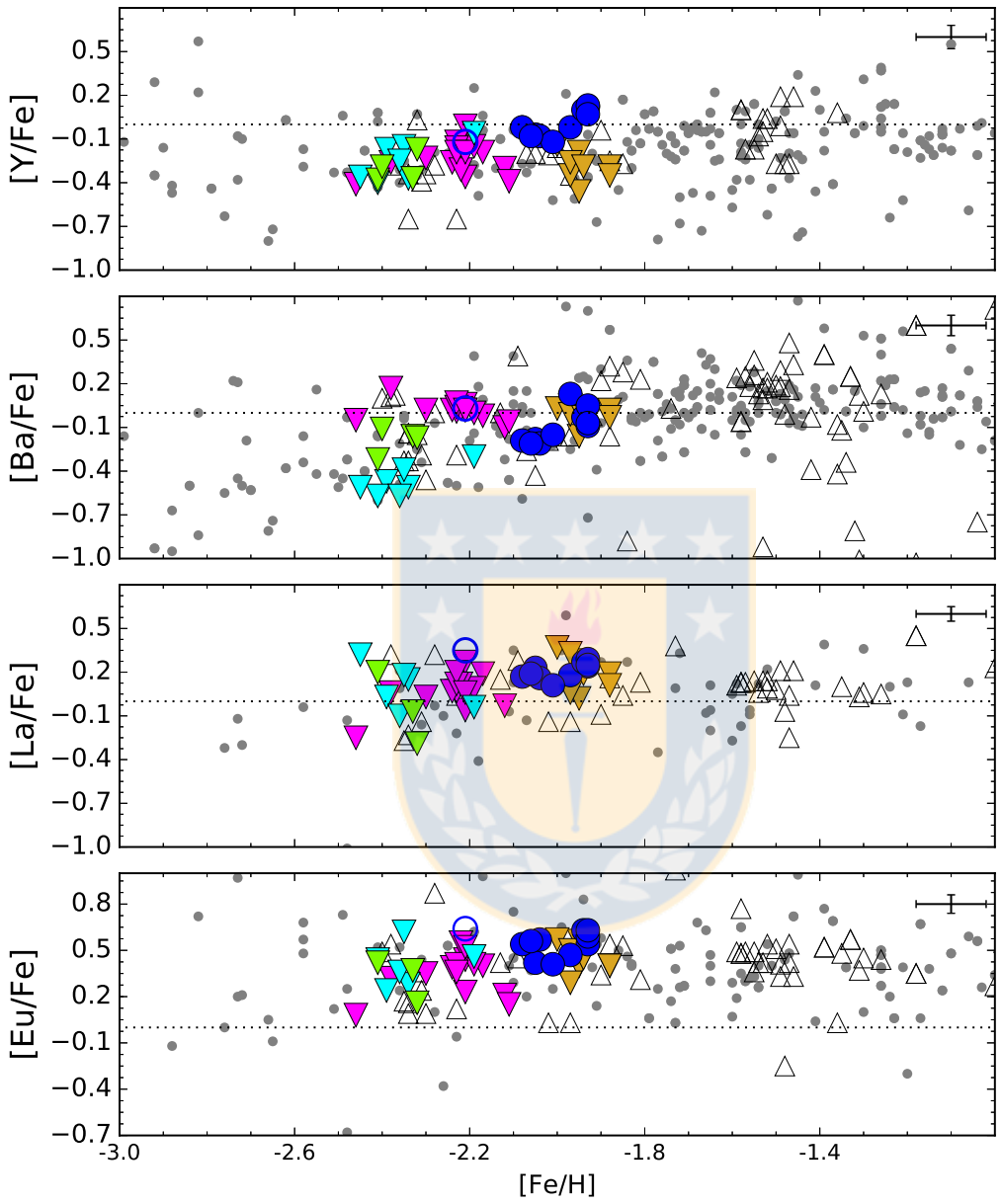

FIGURE 4.5: [Y/Fe], [Ba/Fe], [La/Fe] and [Eu/Fe] ratios versus [Fe/H]. Filled blue circles are our data for NGC 6809. Open blue circle is our data for star #1 (the most metal poor of our sample). Triangles represent different GCs samples: Filled green triangles: NGC 6426 (Hanke et al., 2017). Filled cyan triangles: NGC 4372 (Valenzuela-Calderon et al. in prep). Filled magenta triangles: NGC 4833 (Roederer & Thompson, 2015). Filled golden triangles: NGC 5897 (Koch & McWilliam, 2014). Filled gray circles: Halo and Disc field stars (Fulbright, 2000, Venn et al., 2004). Source: self made.

Our overabundance of La is compared with field Halo giants and GGCs of comparable metallicity (e.g Fulbright, 2000, Roederer & Thompson, 2015, Valenzuela-Calderon et al. in prep) as we can see in Fig. 4.5.

4.1.3.5 Cerium

Cerium shows under-abundant values -0.09 dex and varies from [Ce/Fe] = -0.18 to +0.07 dex. Ce abundances are available only for 10 stars. Our results are in completely agreement with the values found by Pilachowski et al. (1984) (-0.08 dex). Ce abundances doesn't show a significant intrinsic dispersion ($\sigma_{Tot} = 0.05$ versus $\sigma_{Obs} = 0.06$) which is a typical behaviour of GGCs stars.

4.1.3.6 Neodymium

Neodymium abundance is enhanced by +0.15 dex, this value is ~ 0.15 dex lower than the value found by Pilachowski et al. (1984). Nd abundances varies from [Nd/Fe]= +0.22 to +0.43 dex. Our results are in agreement with Nd abundances found for GGCs in the metallicity range around NGC 6809 (e.g NGC 4372, Valenzuela-Calderon et al. in prep). Nd abundance doesn't exhibit intrinsic scatter.

4.1.3.7 Europium

Europium is the most over-abundant n-capture elements ($\sim$0.50 dex) in our sample and also showing a smaller spread ($\sigma_{Obs} = 0.07$). Previous studies in GGCs give very similar results, between +0.30 to +0.50 dex (e.g Hanke et al., 2017, Ivans et al., 2001, Koch & McWilliam, 2014, Pritzl et al., 2005, Ramírez & Cohen, 2003). Europium values found in this paper are also consistent with Eu values in field stars found by Fulbright (2000), Venn et al. (2004). So, we considerer [Eu/Fe] ratios agree with the Galactic trend (see Fig. 4.5).

4.1.3.8 Dysprosium

Mean Dysprosium abundance is enhanced by +0.15 dex, this mean value is normal and compatible with those of other GCs and field Halo stars of the same metallicity (e.g. Hanke et al., 2017, Koch & McWilliam, 2014, Pritzl et al., 2005). Dy abundance varies from [Dy/Fe]= -0.06 to +0.30 dex. Dy abundances are available only for 10 stars. Dy abundances doesn't show a significant intrinsic dispersion ($\sigma_{Tot} = 0.07$ versus $\sigma_{Obs} = 0.09$).

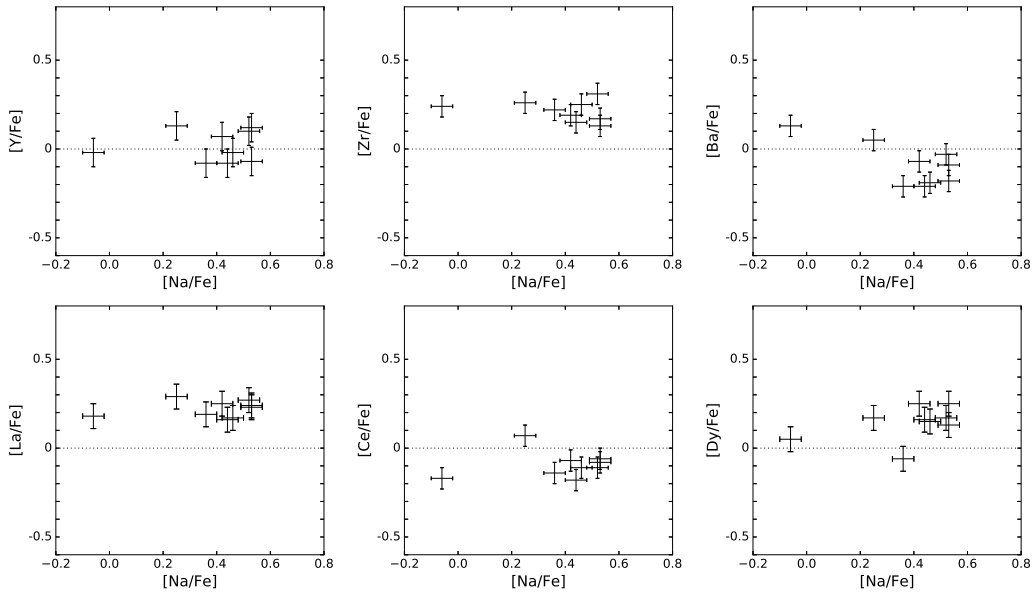

atios versus Na/Fe] [Y/Fe], [Zr/Fe], [Ba/Fe], [La/Fe], [Ce/Fe] and [Dy/Fe] ratios versus [Na/Fe] ratio for our data. Source: self made.

FIGURE 4.6: r

Heavy s-elements La and Ba show no correlation with any of the light elements that exhibiting abundance variations; this is corroborated by the most Na-poor stars in our sample, that do not show clear signs of correlation. Additionally, we plot heavy and light s-elements Ce, Y, Zr, La, Ba and Dy in Figure 4.6 where none of these elements exhibits any significant correlations with the light element Na.

4.1.3.9 [Ba/Eu] ratio versus [Fe/H]

The tracer for r-process nucleosynthesis is Eu, and those for the s-process are Ba and La. In order to know which process is involved in the enrichment of the proto-cluster cloud we plot in Figure 4.7 the [Ba/Eu] ratio as a function of [Fe/H], we found a value of [Ba/Eu] which is very under-solar, and close to pure r-process value [Ba/Eu]=-0.70 (Arlandini et al., 1999). This result is fully compatible with previous analyses in this metallicity regime (Fulbright, 2000, Mashonkina et al., 2003). The previous result strongly suggests that heavy elements in NGC 6809 appear to have been produced by explosive events like core-collapse SNe. The dispersion in [Ba/Eu] ratio is a direct consequence of the dispersion in Ba abundances (again, these dispersions are within the errors).

4.1.4 Light elements

A strong evidence for the existence of Multiple Populations (MPs) in GC is the variations of light elements Na, O, Mg and Al. These elements are involved in the CNO, NeNa,

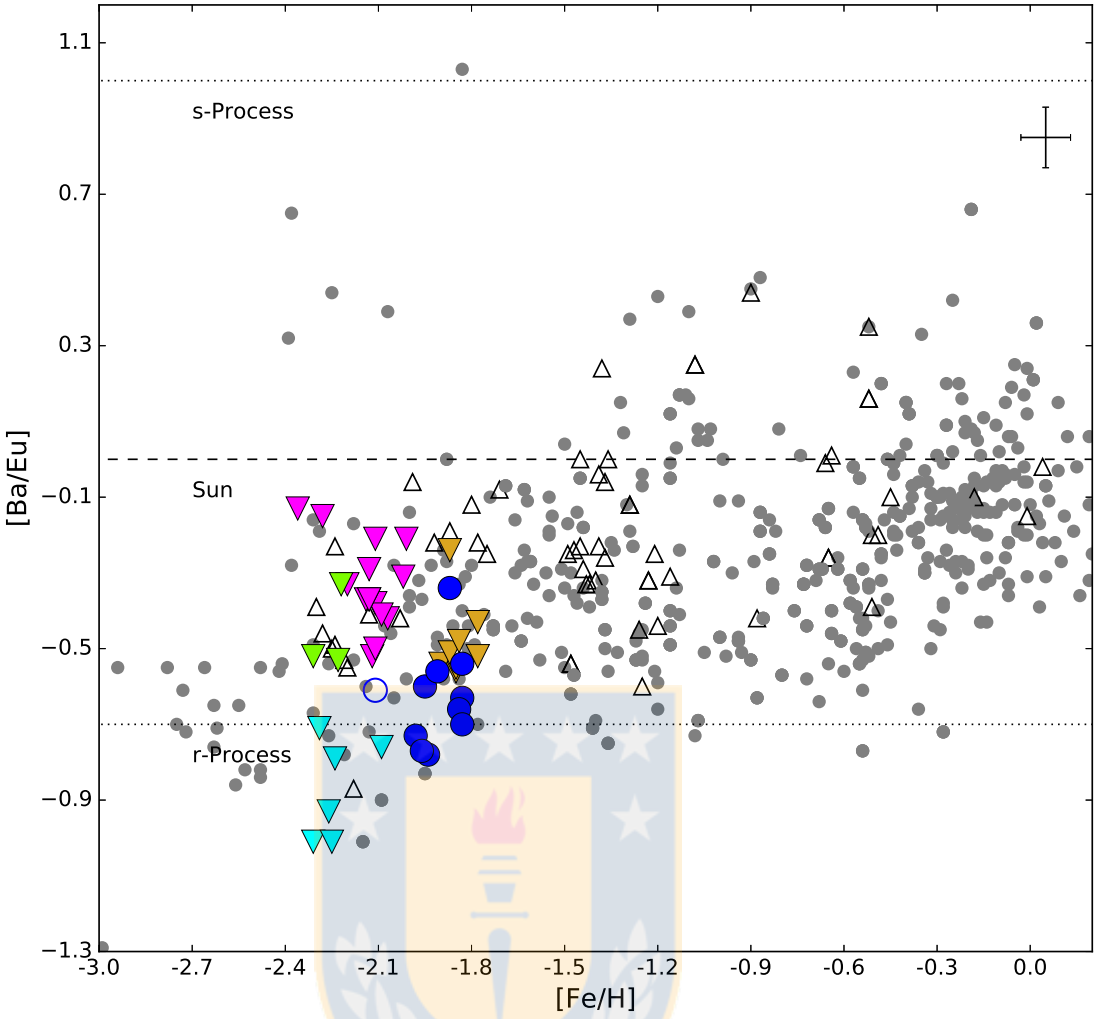

FIGURE 4.7: [Ba/Eu] ratio versus [Fe/H]. Filled blue circle are our data for NGC 6809. Open blue circle is our data for star #1 (the most metal poor of our sample). Triangles represent different GCs samples: Filled magenta triangles: NGC 4833 (Roederer & Thompson, 2015).Filled green triangles: NGC 6426 (Hanke et al., 2017). Filled golden triangles: NGC 5897 (Koch & McWilliam, 2014). Filled gray circles: Halo and Disc field stars (Fulbright, 2000, Ishigaki et al., 2013, Venn et al., 2004). Source: self made.

MgAl cycles of p-capture reactions related to H-burning at high-temperature showing a large star-to-star variations in GC clusters. Field stars with similar metallicities do not share this behaviour. On the other side, GCs contain stars that are characterised by the same abundance pattern observed in field stars of the same metallicity. This indicates that GCs are made up of MPs, as we already mentioned in Section 1. In NGC 6809 these variations are present and in the following section, where we discuss these relations in order to understand the MPs in this cluster.

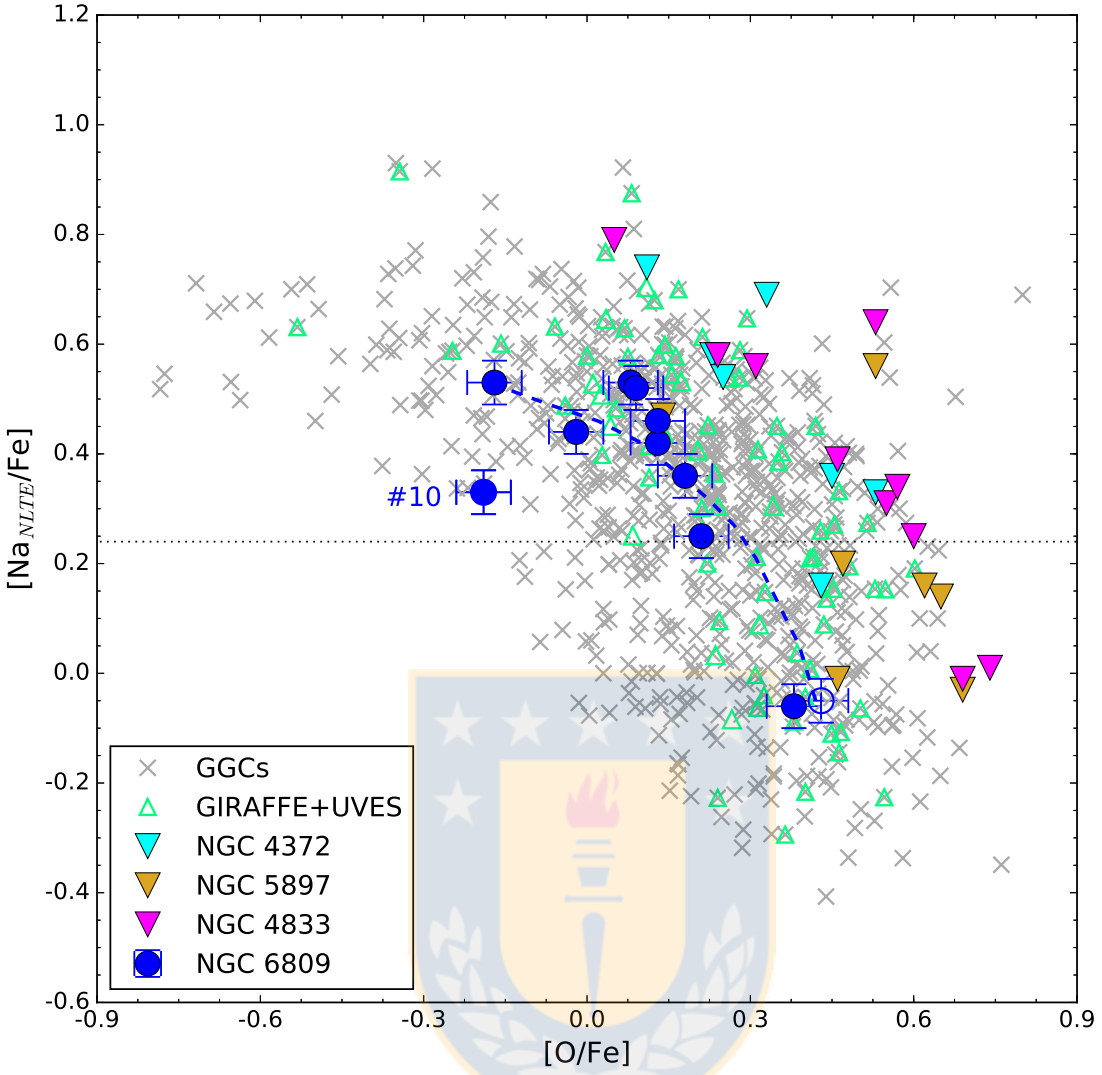

FIGURE 4.8: [Na/Fe] versus [O/Fe]. Filled blue circles are our data for NGC 6809Open blue circle is our data for star #1 (the most metal poor of our sample). Triangles represent different GCs samples: Open pale green triangles represent UVES and GIRAFFE data from Carretta et al. (2009) for NGC 6809. Filled cyan triangles: NGC 4372 (Valenzuela-Calderon et al. in prep). Filled magenta triangles: NGC 4833 (Roederer & Thompson, 2015). Filled golden triangles: NGC 5897 (Koch & McWilliam, 2014). Gray crosses: Galactic Globular Cluster (Carretta et al., 2009). Source: self made.

4.1.4.1 Na-O anticorrelation

Sodium and Oxygen show the well-known anticorrelation found in almost all GCs; this anticorrelation is the main spectroscopic signature of multiple populations in GCs. This feature has been used to define a GC (Carretta et al., 2009, Gratton et al., 2012) and is caused by both proton-capture processes in H-burning at high temperatures through the CNO cycle which depleted Oxygen and the NeNa cycle which enriches Sodium (Arnould et al., 1999). We found a pronounced spread in both Na and O abundances (see Tab. 3.2) revealing the presence of this classical anticorrelation in our cluster.

The only previous study looking for the Na-O anticorrelation in NGC 6809 was performed by Carretta et al. (2009). In Figure 4.8 we plot the [Na/Fe] values as a function of [O/Fe] found in each star of our sample together with those found in the paper recently mentioned. We considered the agreement satisfactory for both Na and O. In comparison with Carretta et al. (2009) our dispersions of Oxygen are higher (σ_{Obs} = 0.18 dex versus σ_{Obs} = 0.11 dex) and our mean value is slightly lower. NLTE corrections were made for Na lines based on the INSPEC [2] database. The mean NLTE corrections obtain for [Na/Fe] is ∼-0.08 dex.

Our Na abundances are 0.05 dex lower than Carretta et al. (2009), but are within the errors. We considerer the agreement satisfactory. Wang et al. (2017) found a mean [Na/Fe] = 0.23 ± 0.15 for the UVES sample and [Na/Fe] = 0.27 ± 0.16 for the GIRAFFE sample, the differences with our work beeing 0.10 and 0.06 dex respectively. This offset probably reflect the difference of ∼0.1 dex we found for the iron with respect to this paper.

If we look at Figure 4.8 it is possible to identify two stars (#1 and #3) in the Na-poor/O-rich region, related to the primordial (P) stellar component (below the dashed horizontal line). On the other hand, a group of Na-rich/O-poor stars provide evidence of second-generation GC stars among the sample.

We fitted the dilution model following Carretta et al. (2009). This model fits well most of the stars, only star #10 is left out. This star does not follow the Na-O anticorrelation described by the rest of the stars in NGC 6809 (see Figure 4.8, left panel). In particular, the O and Na lines in this star are weaker compared with the rest and the S/N is the lowest of the sample (see Table 3.1). We considerer this last the most probable explanation for its low Na content.

4.1.4.2 Mg-Al (anti)correlation

To be able to investigate MPs in NGC 6809, we also need to investigate the anticorrelation between Magnesium and Aluminum. This is useful because the first and second generations lead not only to variations in the Na and O abundance but also a possible variations of the Al and Mg abundances. The origin of this variation in NC 6809 is just the result of the Mg-Al cycle, which converts Mg into Al at a temperature of ∼ 70 million K (Charbonnel & Prantzos, 2006).

In our sample Al is overabundant with a high average value of ⟨[Al/Fe]⟩ = +0.86 dex. Both elements show an internal dispersion, being more clear for Aluminum (σ_{Obs} = 0.34

[2] http://inspect.coolstars19.com/index.php?n=Main.HomePage

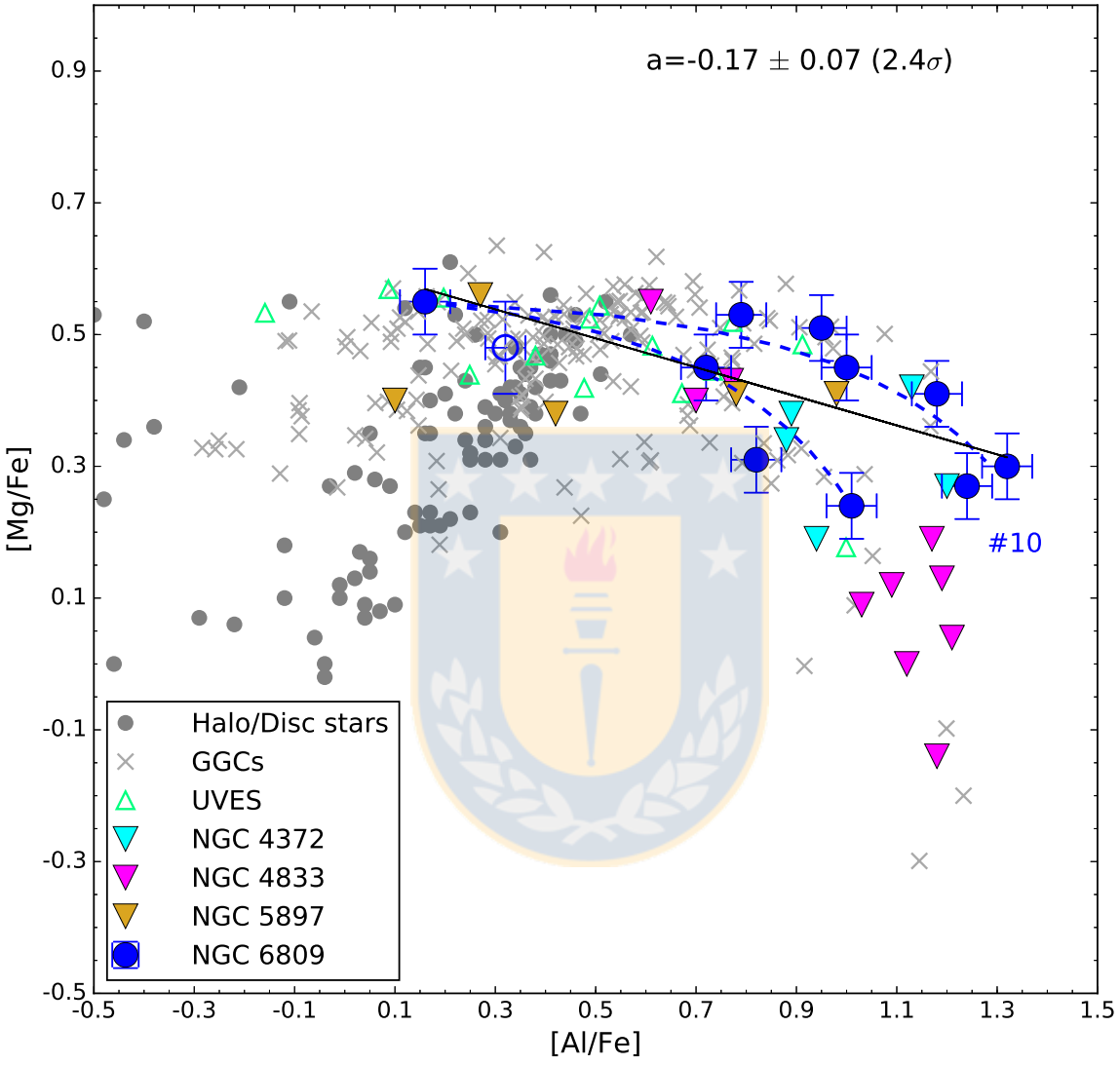

FIGURE 4.9: [Mg/Fe] versus [Al/Fe]. Filled blue circles are our data for NGC 6809. Open blue circle is our data for star #1 (the most metal poor of our sample). Triangles represent different GCs samples: Open pale green triangles represent UVES and GIRAFFE data from Carretta et al. (2009) for NGC 6809. Filled cyan triangles: NGC 4372 (Valenzuela-Calderon et al. in prep). Filled magenta triangles: NGC 4833 (Roederer & Thompson, 2015). Filled golden triangles: NGC 5897 (Koch & McWilliam, 2014). Gray crosses: Galactic Globular Cluster (Carretta et al., 2009). Filled gray circles: Halo and Disc field stars (Cayrel et al., 2004, Fulbright, 2000). Black dash line is the best fit for our sample. Source: self made.

v/s $\sigma_{Tot} = 0.07$) than for Magnesium ($\sigma_{Obs} = 0.10$ v/s $\sigma_{Tot} = 0.04$). This is not surprising since in general Aluminum abundances show an high spread in almost all galactic GCs, especially in those with a metallicity lower than [Fe/H]=-1.1 dex (Carretta et al., 2009, Mészáros et al., 2015, Pancino et al., 2017). We found that the differences between our most Al-rich and Al-poor star is about ∼1.10 dex, on the other hand, the difference between our most Mg-rich and Mg-poor stars is ∼0.30 dex. Left panel of Figure 4.8 display the [Mg/Fe] ratio as a function of [Al/Fe] ratio together with data from Carretta et al. (2009), Halo and Disc field stars and GC having metallicity similar to NGC 6809. The anticorrelation found is clear. Additionally, we perform a linear fit to the sample; this fit has a slope of a = -0.17 with an error of ±0.07. This corresponds to a significance of the slope of 2.4σ, that we consider statistically significant. However it appears to us that a linear fit is not the best interpretation of the data. If we combine our results with those from other GCd, we see quite clearly that in Figure 4.8 (right panel), two Mg-Al relation appears. These are indicated by the two dilution models we fit to the data. In NGC 6809 both are present, while in other clusters like NGC 4833 only one of them is found. This could indicate that in NGC 6809 two kind of polluters are responsible for the MP-phenomenon. More data are required to confirm this behaviour. With all the aforementioned evidence, we can confirm the existence of a Mg-Al anti-correlation in NGC 6809 for the first time. Carretta et al. (2009) find this pattern only in massive GCs (e.g NGC 2808, 6388 and NGC 6441), in metal-poor GC (e.g NGC 6752), or both (NGC 7078 = M15). Despite our cluster show a typical mass ($10^5 M_\odot$) for a GGC and it is one of the most metal-poor clusters studied to date, they did not find clear signs of an anti-correlation in NGC 6809 as we do. However, they mean abundances are in agreement with ours.

4.1.4.3 Na-Al correlation

Al is expected to correlate with elements enhanced by proton-capture reactions (e.g. Na). Several authors found a correlation between Aluminum and Sodium (e.g Carretta et al., 2009, Ivans et al., 2001, Shetrone, 1996). This anti-correlation is predicted to be simultaneously enhanced when the NeNa and MgAl cycles are both acting. Features of these elements are in general easier to measure, and the associated changes in abundance are usually larger than for O and Mg.

In figure 4.10 we plot [Al/Fe] ratio as a function of [Na/Fe] ratio. From this figure, it is clear that our stars do not follow the typical Halo and Disc trend which has [Al/Fe]≅0.0 at [Fe/H]∼ -2.0. The interesting point is that our correlation is not continuous, sharing the same behaviour show in both Na-O and Mg-Al anticorrelations where our sample is categorised into two groups: two stars (#1 and #3) with low-Na and low-Al and nine

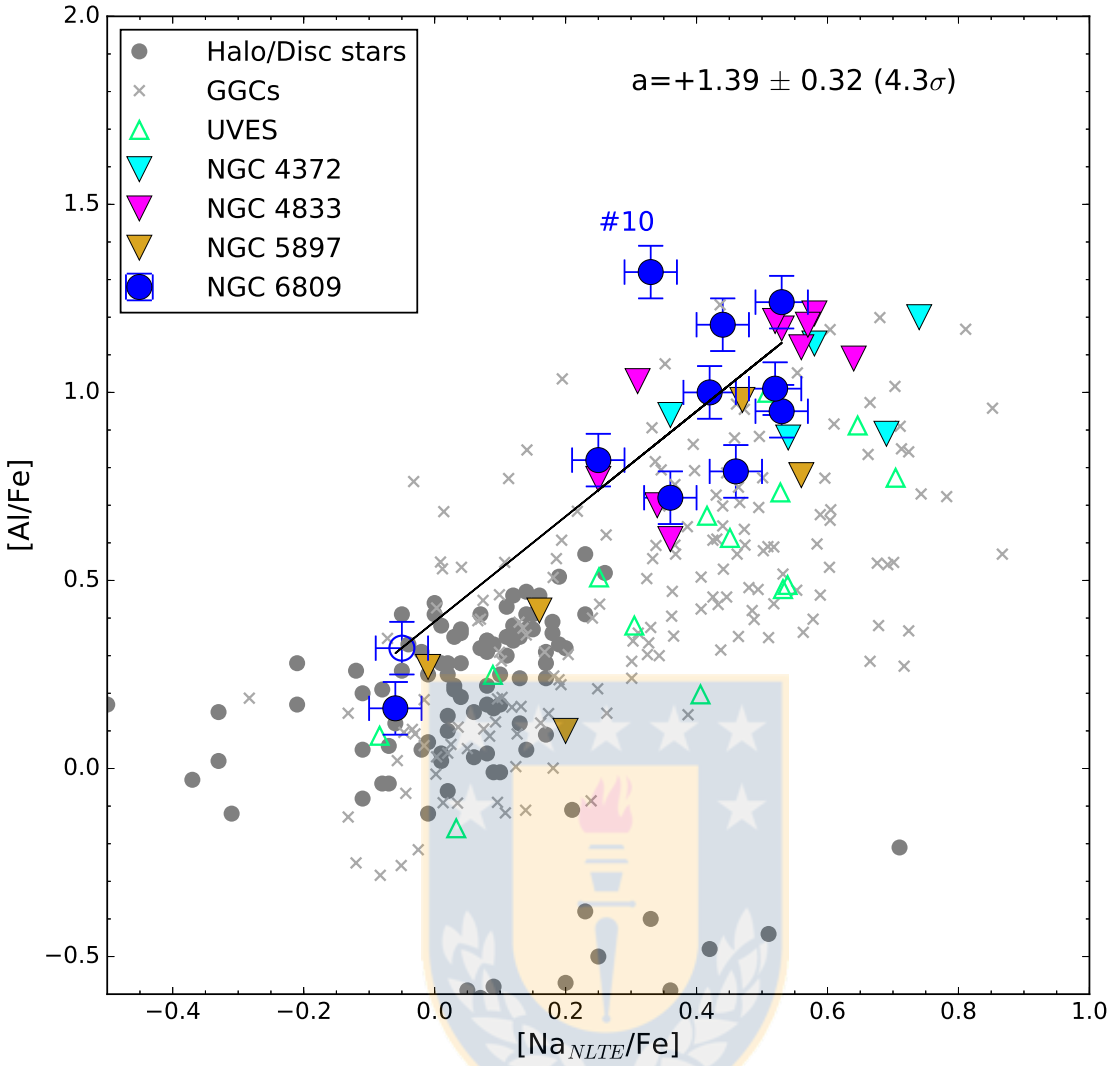

FIGURE 4.10: [Al/Fe] versus [Na/Fe]. Filled blue circles are our data for NGC 6809. Open blue circle is our data for star #1 (the most metal poor of our sample). Triangles represent different GCs samples: Open pale green triangles represent UVES and GIRAFFE data from Carretta et al. (2009) for NGC 6809. Filled cyan triangles: NGC 4372 (Valenzuela-Calderon et al. in prep). Filled magenta triangles: NGC 4833 (Roederer & Thompson, 2015). Filled golden triangles: NGC 5897 (Koch & McWilliam, 2014). Gray crosses: Galactic Globular Cluster (Carretta et al., 2009). Filled gray circles: Halo and Disc field stars (Cayrel et al., 2004, Fulbright, 2000). Black dash line is the best fit for our sample. Source: self made.

stars with high-Na and high-Al. We perform the best-fit to our sample, this fit has a slope of a = +1.39 with an error of ±0.32 this corresponds to a significance of the slope of 4.3σ. The correlation between Sodium and Aluminum is clear.

Chapter 5

Discusion and Conclusions

We have analysed UVES spectra of 11 stars of the Halo galactic Globular Cluster NGC 6809. We use two techniques: The classical EW method was used for unblended lines, otherwise we applied the spectrum-synthesis method. We measured a mean cluster heliocentric radial velocity of $\langle RV_H \rangle = 174.7 \pm 3.26$ kms^{-1}. For all the stars, we were able to perform a detailed chemical composition analysis we found that:

α-elements: NGC 6809 is α-enhanced by $[\alpha/\mathrm{Fe}] = +0.40 \pm 0.04$. Mg, Si, Ca and Ti are over-abundant. This Cluster follows the same trend as galactic Globular Clusters and Halo field stars. According to our results, NGC 6809 suffered a rapid chemical evolution dominated by SNeII.

Iron and iron-peak elements: We found $\langle$[Fe/H]$\rangle$ = -2.01 $\pm$ 0.02 (error on the mean), in good agreement with previous studies Carretta et al. (2009), Wang et al. (2017) and Harris (1996). No significant spread of iron is found in this work. The Fe-peak elements show good agreements with other Globular Clusters and Halo field stars. No evidence of internal dispersion of any of these elements.

Neutron capture elements: Since light and heavy s-elements do not show abundances variations with light elements, we ruled out the possibility of AGB stars as polluters of the second generations of stars. On the other hand, [Ba/Eu] ratio confirms a dominant contribution of the r-process.

Light elements: We found that NGC 6809 exhibits the classical light element abundance variations associated with globular clusters, including a right O-Na anti-correlation and for the first time we confirmed the presence of a Mg-Al anti-correlation. We also found a Na-Al correlation. Al spread is the highest among the light elements. In our analysis, it is possible to observe two groups of stars: Two Na-poor/O-rich and Nine Na-rich/O-poor. The same behaviour is observed in the Mg-Al and Na-Al (anti)correlations.

Bibliography

Alcaino G., 1975, A&AS, 22, 193

Aller L. H., Greenstein J. L., 1960, ApJS, 5, 139

Alonso A., Arribas S., Martínez-Roger C., 1999, A&AS, 140, 261

Arlandini C., Käppeler F., Wisshak K., Gallino R., Lugaro M., Busso M., Straniero O., 1999, ApJ, 525, 886

Arnould M., Goriely S., Jorissen A., 1999, A&A, 347, 572

Barbuy B., Spite F., Spite M., 1985, A&A, 144, 343

Barklem P. S., Christlieb N., Beers T. C., Hill V., Bessell M. S., Holmberg J., Marsteller B., Rossi S., Zickgraf F.-J., Reimers D., 2005, A&A, 439, 129

Battistini C., Bensby T., 2015, A&A, 577, A9

Bensby T., Feltzing S., Lundström I., Ilyin I., 2005, A&A, 433, 185

Boyles J., Lorimer D. R., Turk P. J., Mnatsakanov R., Lynch R. S., Ransom S. M., Freire P. C., Belczynski K., 2011, The Astrophysical Journal, 742, 51

Buzzoni A., Patelli L., Bellazzini M., Pecci F. F., Oliva E., 2010, MNRAS, 403, 1592

Carretta E., 2003, Memorie della Societa Astronomica Italiana Supplementi, 3, 90

Carretta E., Bragaglia A., Gratton R., D'Orazi V., Lucatello S., 2009, A&A, 508, 695

Carretta E., Bragaglia A., Gratton R., Lucatello S., 2009, A&A, 505, 139

Carretta E., Bragaglia A., Gratton R., Lucatello S., Bellazzini M., D'Orazi V., 2010, ApJL, 712, L21

Carretta E., Bragaglia A., Gratton R. G., D'Orazi V., Lucatello S., Sollima A., 2014, A&A, 561, A87

Carretta E., Bragaglia A., Gratton R. G., Lucatello S., Catanzaro G., Leone F., Bellazzini M., Claudi R., D'Orazi V., Momany Y., Ortolani S., Pancino E., Piotto G., Recio-Blanco A., Sabbi E., 2009, A&A, 505, 117

Carretta E., Bragaglia A., Gratton R. G., Recio-Blanco A., Lucatello S., D'Orazi V., Cassisi S., 2010, A&A, 516, A55

Cayrel R., Depagne E., Spite M., Hill V., Spite F., François P., Plez B., Beers T., Primas F., Andersen J., Barbuy B., Bonifacio P., Molaro P., Nordström B., 2004, A&A, 416, 1117

Charbonnel C., Prantzos N., 2006, ArXiv Astrophysics e-prints

Cohen J. G., Briley M. M., Stetson P. B., 2002, AJ, 123, 2525

Cottrell P. L., Da Costa G. S., 1981, ApJL, 245, L79

D'Antona F., Caloi V., Montalbán J., Ventura P., Gratton R., 2002, A&A, 395, 69

de Mink S. E., Pols O. R., Langer N., Izzard R. G., 2009, A&A, 507, L1

Decressin T., Charbonnel C., Siess L., Palacios A., Meynet G., Georgy C., 2009, A&A, 505, 727

Decressin T., Meynet G., Charbonnel C., Prantzos N., Ekström S., 2007, A&A, 464, 1029

Denisenkov P. A., Denisenkova S. N., 1989, Astronomicheskij Tsirkulyar, 1538, 11

Denisenkov P. A., Denisenkova S. N., 1990, Soviet Astronomy Letters, 16, 275

Denissenkov P. A., Hartwick F. D. A., 2014, MNRAS, 437, L21

Denissenkov P. A., Herwig F., 2003, ApJL, 590, L99

Dotter A., Sarajedini A., Anderson J., Aparicio A., Bedin L. R., Chaboyer B., Majewski S., Marín-Franch A., Milone A., Paust N., Piotto G., Reid I. N., Rosenberg A., Siegel M., 2010, ApJ, 708, 698

Fulbright J. P., 2000, AJ, 120, 1841

Goldsbury R., Richer H. B., Anderson J., Dotter A., Sarajedini A., Woodley K., 2010, AJ, 140, 1830

Gonzalez O. A., Rejkuba M., Zoccali M., Hill V., Battaglia G., Babusiaux C., Minniti D., Barbuy B., Alves-Brito A., Renzini A., Gomez A., Ortolani S., 2011, A&A, 530, A54

Gratton R., Sneden C., Carretta E., 2004, ARA&A, 42, 385

Gratton R. G., Bonifacio P., Bragaglia A., Carretta E., Castellani V., Centurion M., Chieffi A., Claudi R., Clementini G., D'Antona F., Desidera S., 2001, A&A, 369, 87

Gratton R. G., Carretta E., Bragaglia A., 2012, **??**jnlA&A Rev., 20, 50

Gratton R. G., Carretta E., Eriksson K., Gustafsson B., 1999, A&A, 350, 955

Gratton R. G., Sneden C., 1988, A&A, 204, 193

Gratton R. G., Sneden C., 1991, A&A, 241, 501

Hanke M., Koch A., Hansen C. J., McWilliam A., 2017, A&A, 599, A97

Harris W. E., 1975, ApJS, 29, 397

Harris W. E., 1996, AJ, 112, 1487

Harris W. E., 2001, Globular Cluster Systems. p. 223

Harris W. E., 2010, ArXiv e-prints

Ishigaki M. N., Aoki W., Chiba M., 2013, ApJ, 771, 67

Ivans I. I., Kraft R. P., Sneden C., Smith G. H., Rich R. M., Shetrone M., 2001, AJ, 122, 1438

James G., François P., Bonifacio P., Carretta E., Gratton R. G., Spite F., 2004, A&A, 427, 825

Johnson C. I., Caldwell N., Rich R. M., Walker M. G., 2017, AJ, 154, 155

Johnson C. I., Rich R. M., Pilachowski C. A., Caldwell N., Mateo M. L., Ira Bailey J., Crane J. D., 2016, in American Astronomical Society Meeting Abstracts Vol. 227 of American Astronomical Society Meeting Abstracts, NGC 6273: Towards Defining A New Class of Galactic Globular Clusters?. p. 240.03

Kaluzny J., Thompson I. B., Krzeminski W., Zloczewski K., 2010, ACTAA, 60, 245

Kayser A., Hilker M., Grebel E. K., Willemsen P. G., 2008, A&A, 486, 437

Koch A., McWilliam A., 2014, A&A, 565, A23

Kurucz R. L., 1970, SAO Special Report, 309

Lane R. R., Kiss L. L., Lewis G. F., Ibata R. A., Siebert A., Bedding T. R., Székely P., Szabó G. M., 2011, A&A, 530, A31

Lanzoni B., Dalessandro E., Perina S., Ferraro F. R., Rood R. T., Sollima A., 2007, ApJ, 670, 1065

Lee J.-W., Carney B. W., 2002, AJ, 124, 1511

Lee S.-W., 1977, A&AS, 29, 1

Marino A. F., Milone A. P., Karakas A. I., Casagrande L., Yong D., Shingles L., Da Costa G., Norris J. E., Stetson P. B., Lind K., Asplund M., Collet R., Jerjen H., Sbordone L., Aparicio A., Cassisi S., 2015, MNRAS, 450, 815

Marino A. F., Milone A. P., Piotto G., Villanova S., Gratton R., D'Antona F., Anderson J., Bedin L. R., Bellini A., Cassisi S., Geisler D., Renzini A., Zoccali M., 2011, ApJ, 731, 64

Marino A. F., Villanova S., Piotto G., Milone A. P., Momany Y., Bedin L. R., Medling A. M., 2008, A&A, 490, 625

Mashonkina L., Gehren T., Travaglio C., Borkova T., 2003, A&A, 397, 275

McWilliam A., Preston G. W., Sneden C., Searle L., 1995, AJ, 109, 2757

Mészáros S., Martell S. L., Shetrone M., Lucatello S., Troup N. W., Bovy J., Cunha K., García-Hernández D. A., 2015, AJ, 149, 153

Minniti D., Geisler D., Peterson R. C., Claria J. J., 1993, ApJ, 413, 548

Mucciarelli A., Merle T., Bellazzini M., 2017, A&A, 600, A104

Nissen P. E., Akerman C., Asplund M., Fabbian D., Kerber F., Kaufl H. U., Pettini M., 2007, A&A, 469, 319

Nissen P. E., Gustafsson B., Edvardsson B., Gilmore G., 1994, A&A, 285, 440

Nomoto K., Thielemann F.-K., Wheeler J. C., 1984, ApJL, 279, L23

Norris J., 1987, ApJL, 313, L65

Olech A., Kaluzny J., Thompson I. B., Pych W., Krzeminski W., Schwarzenberg-Czerny A., 1999, AJ, 118, 442

Osborn W., 1971, The Observatory, 91, 223

Pancino E., Rejkuba M., Zoccali M., Carrera R., 2010, A&A, 524, A44

Pancino E., Romano D., Tang B., Tautvaišienė G., Casey A. R., Gruyters P., Geisler D., San Roman I., Randich S., 2017, A&A, 601, A112

Pilachowski C. A., Sneden C., Green E. M., 1984, PASP, 96, 932

Piotto G., Milone A. P., Bedin L. R., Anderson J., King I. R., Marino A. F., Nardiello D., Aparicio A., Barbuy B., 2015, AJ, 149, 91

Prantzos N., Charbonnel C., 2006, A&A, 458, 135

Prantzos N., Charbonnel C., Iliadis C., 2007, A&A, 470, 179

Pritzl B. J., Venn K. A., Irwin M., 2005, AJ, 130, 2140

Prochaska J. X., McWilliam A., 2000, ApJL, 537, L57

Pryor C., McClure R. D., Fletcher J. M., Hesser J. E., 1991, AJ, 102, 1026

Ramírez S. V., Cohen J. G., 2002, AJ, 123, 3277

Ramírez S. V., Cohen J. G., 2003, AJ, 125, 224

Renzini A., 2008, MNRAS, 391, 354

Richter P., Hilker M., Richtler T., 1999, A&A, 350, 476

Roederer I. U., Mateo M., Bailey J. I., Spencer M., Crane J. D., Shectman S. A., 2016, MNRAS, 455, 2417

Roederer I. U., Preston G. W., Thompson I. B., Shectman S. A., Sneden C., Burley G. S., Kelson D. D., 2014, AJ, 147, 136

Roederer I. U., Thompson I. B., 2015, MNRAS, 449, 3889

Rozyczka M., Kaluzny J., Thompson I. B., Rucinski S. M., Pych W., Krzeminski W., 2013, ACTAA, 63, 67

Salaris M., Weiss A., 2002, A&A, 388, 492

Sariya D. P., Yadav R. K. S., Bellini A., 2012, A&A, 543, A87

Shetrone M. D., 1996, AJ, 112, 1517

Simmerer J., Sneden C., Ivans I. I., Kraft R. P., Shetrone M. D., Smith V. V., 2003, AJ, 125, 2018

Smith G. H., Norris J., 1982, ApJ, 254, 149

Sneden C., 1973, ApJ, 184, 839

Sneden C., 2004, MEMSAI, 75, 267

Sneden C., Gratton R. G., Crocker D. A., 1991, A&A, 246, 354

Sobeck J. S., Ivans I. I., Simmerer J. A., Sneden C., Hoeflich P., Fulbright J. P., Kraft R. P., 2006, AJ, 131, 2949

Thompson R. B., Thompson B. F., 2007, Illustrated Guide to Astronomical Wonders, first edn. O'Reilly

Tinsley B. M., 1979, ApJ, 229, 1046

Trager S. C., Djorgovski S., King I. R., 1993, in Djorgovski S. G., Meylan G., eds, Structure and Dynamics of Globular Clusters Vol. 50 of Astronomical Society of the Pacific Conference Series, Structural Parameters of Galactic Globular Clusters. p. 347

Trager S. C., King I. R., Djorgovski S., 1995, AJ, 109, 218

Vargas Álvarez C. A., Sandquist E. L., 2007, AJ, 134, 825

Venn K. A., Irwin M., Shetrone M. D., Tout C. A., Hill V., Tolstoy E., 2004, AJ, 128, 1177

Ventura P., D'Antona F., 2011, MNRAS, 410, 2760

Ventura P., D'Antona F., Mazzitelli I., Gratton R., 2001, ApJL, 550, L65

Ventura P., Di Criscienzo M., Carini R., D'Antona F., 2013, MNRAS, 431, 3642

Villanova S., Geisler D., 2011, A&A, 535, A31

Villanova S., Geisler D., Carraro G., Moni Bidin C., Muñoz C., 2013, ApJ, 778, 186

Villanova S., Geisler D., Gratton R. G., Cassisi S., 2014, ApJ, 791, 107

Wallerstein G., 1962, ApJS, 6, 407

Wang Y., Primas F., Charbonnel C., Van der Swaelmen M., Bono G., Chantereau W., Zhao G., 2017, ArXiv e-prints

Webbink R. F., 1985, in Goodman J., Hut P., eds, Dynamics of Star Clusters Vol. 113 of IAU Symposium, Structure parameters of galactic globular clusters. pp 541–577

Woosley S. E., Weaver T. A., 1995, ApJS, 101, 181

Zhao G., Magain P., 1990, A&A, 238, 242

Zinn R., 1977, ApJ, 218, 96

Zloczewski K., Kaluzny J., Thompson I. B., 2011, MNRAS, 414, 3711